

4

DTIC FILE COPY

GL-TR-89-0178
ENVIRONMENTAL RESEARCH PAPERS, NO. 1034

AD-A218 116

Study of Possible Solar Heating Effects on
Thermosonde Probes — Error Analysis

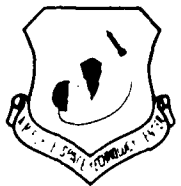
JAMES H. BROWN,
EDMOND DEWAN,
EDMUND MURPHY,
PETER THOMAS



10 July 1989



Approved for public release;
Distribution unlimited



DTIC
ELECTE
FEB 13 1990
S E D
co




OPTICAL AND INFRARED TECHNOLOGY DIVISION PROJECT 7670

GEOPHYSICS LABORATORY
HANSCOM AFB, MA 01731-5000

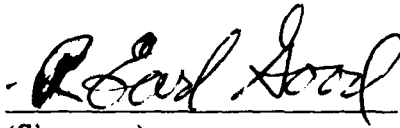
90 02 10 1989

"This technical report has been reviewed and is approved for publication"



for (Signature)
Donald E. Bedo, Chief
Atmospheric Optics Branch

FOR THE COMMANDER



(Signature)
R. Earl Good, Director
Optical and Infrared Technology Division

This report has been reviewed by the ESD Public Affairs Office (PA) and is releasable to the National Technical Information Service (NTIS).

Qualified requestors may obtain additional copies from the Defense Technical Information Center. All others should apply to the National Technical Information Service.

If your address has changed, or if you wish to be removed from the mailing list, or if the addressee is no longer employed by your organization, please notify GL(AFSC)/DAA, Hanscom AFB, MA 01731. This will assist us in maintaining a current mailing list.

Do not return copies of this report unless contractual obligations or notices on a specific document requires that it be returned.

REPORT DOCUMENTATION PAGE				Form Approved OMB No. 0704-0188	
1a. REPORT SECURITY CLASSIFICATION Unclassified		1b. RESTRICTIVE MARKINGS			
2a. SECURITY CLASSIFICATION AUTHORITY		3. DISTRIBUTION / AVAILABILITY OF REPORT Approved for public release; Distribution Unlimited.			
2b. DECLASSIFICATION / DOWNGRADING SCHEDULE					
4. PERFORMING ORGANIZATION REPORT NUMBER(S) GL-TR-89-0178 ERP, NO. 1034		5. MONITORING ORGANIZATION REPORT NUMBER(S)			
6a. NAME OF PERFORMING ORGANIZATION Geophysics Laboratory		6b. OFFICE SYMBOL (If applicable) OPA		7a. NAME OF MONITORING ORGANIZATION	
6c. ADDRESS (City, State, and ZIP Code) Hanscom AFB Massachusetts 01731-5000		7b. ADDRESS (City, State, and ZIP Code)			
8a. NAME OF FUNDING / SPONSORING ORGANIZATION		8b. OFFICE SYMBOL (If applicable)		9. PROCUREMENT INSTRUMENT IDENTIFICATION NUMBER	
8c. ADDRESS (City, State, and ZIP Code)		10. SOURCE OF FUNDING NUMBERS			
		PROGRAM ELEMENT NO. 62101F	PROJECT NO. 7670	TASK NO. 15	WORK UNIT ACCESSION NO. 15
11. TITLE (Include Security Classification) Study of Possible Solar Heating Effects on Thermosonde Probes - Error Analysis					
12. PERSONAL AUTHOR(S) Brown, James H., Dewan, Edmond, Murphy, Edmund, Thomas, Peter					
13a. TYPE OF REPORT Scientific, Interim		13b. TIME COVERED FROM _____ TO _____		14. DATE OF REPORT (Year, Month, Day) 1989 July 10	
				15. PAGE COUNT 74	
16. SUPPLEMENTARY NOTATION					
17. COSATI CODES			18. SUBJECT TERMS (Continue on reverse if necessary and identify by block number)		
FIELD	GROUP	SUB-GROUP	Optical Turbulence, C_n^2 , Thermosonde, Turbulence Diurnal Effect		
19. ABSTRACT (Continue on reverse if necessary and identify by block number) Thermosonde data reveals a diurnal daytime shift in measured levels of C_n^2 in the free atmosphere. The shift is manifested in two ways. First, an apparent offset in the smallest measured values of C_n^2 exists. Secondly, the curve of the average profile shows an enhancement over nighttime profiles. Related optical and radar measurements have indicated that differences between day and night probably exist, but because of limited instrumental resolution and altitude capabilities those results are inconclusive. Several hypotheses have been put forward in this paper concerning possible instrumental or solar based sources of data contamination. We have examined the possibility that solar radiation causes probe heating with subsequent instrumental effects. Calculation, computer simulation, and direct measurements have shown that the sun heats the body of the probe sensor a couple of degrees above the ambient and that the level of heating depends upon the solar aspect angle and magnitude.					
20. DISTRIBUTION / AVAILABILITY OF ABSTRACT <input checked="" type="checkbox"/> UNCLASSIFIED / UNLIMITED <input type="checkbox"/> SAME AS RPT. <input type="checkbox"/> DTIC USERS			21. ABSTRACT SECURITY CLASSIFICATION Unclassified		
22a. NAME OF RESPONSIBLE INDIVIDUAL James H. Brown			22b. TELEPHONE (Include Area Code) (617) 377-4412		22c. OFFICE SYMBOL OPA

BLOCK #19 (continued)

and direction of air flow over the probe. Small number statistics have also indicated some correlation between the solar angle and the baseline shift. However, additional calculations, turbulence simulations, in-situ measurements, and direct laboratory experiments do not support the instrumental data contamination hypothesis. A small but insignificant AC type effect can result from improper probe geometry or probe mismatch together with a coupling of solar heating with velocity turbulence. Transient and DC type effects can occur, but measured, processed, and transmitted root mean square C^2 information is not likely to contain instrumental contamination.

C^2
(C square R)

Accession For	
NTIS GRA&I	<input checked="" type="checkbox"/>
DTIC TAB	<input type="checkbox"/>
Unannounced	<input type="checkbox"/>
Justification	
By _____	
Distribution/	
Availability Codes	
Dist	Avail and/or Special
A-1	



Contents

1. INTRODUCTION	1
2. HEAT TRANSFER CONSIDERATIONS	3
2.1 Cross-Flow Convective Transfer in the Presence of Radiative Heat Transfer	3
2.2 Parallel-Flow Convective Transfer for a Cylinder	7
2.3 Effects Due to Solar Radiation Incidence Angle	10
3. THEORETICAL AND EXPERIMENTAL VALUES OF ΔT	11
4. EVIDENCE FOR ΔT EFFECTS ON C_T^2 MEASUREMENTS	15
4.1 Baseline Shift (BLS)	16
4.2 Correlation between C_T^2 and ΔT	19
4.3 Discussion	28
5. TESTS FOR THE DETERMINATION OF THE REALITY OF THE DIURNAL EFFECTS	30
5.1 Possible Mechanism for Observed BLS	31
5.2 Special In-Situ Balloon Experiments	35
5.3 Low Density Chamber Experiments	49
6. CONCLUSIONS	55
REFERENCES	57

Contents

APPENDIX

61

Illustrations

1. Thermosonde Probe, Diagram.	2
2. Perspective Drawing, Thermosonde Probe Support and Velocity Vector.	8
3. Increase in Probe Temperature as a Function of Altitude, Calculated and Measured Values for Black, White, and Unpainted Probes, from Tables 9B and 10.	13
4. Increase in Probe Temperature as a Function of Altitude, Calculated for a 90° Aspect Angle.	14
5. Increase in Probe Temperature as a Function of Altitude, Calculated for 6:00AM and 8:00AM.	14
6. Distribution of Wire-Air Temperature as Function of Distance along Wire.	16
7a. Thermosonde Measured Values of C_n^2 as a Function of Altitude, Raw Data for Nighttime Profile M6410.	17
7b. Thermosonde Measured Values of C_n^2 as a Function of Altitude, Raw Data for Daytime Profile M6388.	18
8a. Gaussian Averaged Profile for Flight M6483, $\sigma = 40$ meters.	20
8b. 500 Meter Running Average Profile for Flight M6483.	21
8c. 2500 Meter Box Average C_T^2 Profile for Flight M6483.	22
9. Average Measurements and Regression Curve of C_T^2 as a Function of Calculated Temperature Increase for Unpainted Stainless Steel Probes.	26

Illustrations

10. Average Measurements and Regression Curve of C_1^2 as a Function of Calculated Temperature Increase for White Painted Probes.	29
11. Random Number Computer Simulation of Difference between Air and Wire RMS Temperature Variations between Probes as a Function of RMS Air Temperature Variation with Random Numbers Uncorrelated in Terms of Fluctuations in Temperature and Velocity at the Probes.	34
12. Random Number Computer Simulation of Difference between Air and Wire RMS Temperature Variations between Probes as a Function of RMS Air Temperature Variation with Random Numbers Correlated in Terms of Fluctuations in Temperature and Velocity at the Probes.	34
13. Thermosonde C_n^2 Profile (L0948) as a Function of Altitude for Plain, Unpainted Stainless Steel Probes.	36
14. Thermosonde C_n^2 Profile (L0949) as a Function of Altitude for Taped but Unpainted Stainless Steel Probes.	37
15. Thermosonde C_n^2 Profile (L0957) as a Function of Altitude for Taped but Unpainted Stainless Steel Probes.	38
16. Thermosonde C_n^2 Profile (L0961) as a Function of Altitude for Taped and White Painted Stainless Steel Probes.	39
17. Thermosonde C_n^2 Profile (L4023) as a Function of Altitude for Black Painted Stainless Steel Probes.	40

Illustrations

18. Thermosonde C_n^2 Profile (L4021) as a Function of Altitude for Taped and White Painted Stainless Steel Probes.	41
19. Thermosonde C_n^2 Profile (L4024) as a Function of Altitude for Black Painted Stainless Steel Probes.	42
20. Thermosonde C_n^2 Profile (L4020) as a Function of Altitude for One Black Painted Stainless Steel Probes and One Taped and White Painted Stainless Steel Probe.	44
21. Thermosonde C_n^2 Profile (L1016) as a Function of Altitude for Long Wire Unpainted Stainless Steel Probes.	45
22. Thermosonde C_n^2 Profile (L0952) as a Function of Altitude for a Very Long Balloon Train and Thermosonde Having Plain Unpainted Stainless Steel Probes.	46
23. Thermosonde C_n^2 Profile (L1019) as a Function of Altitude for Fixed Low Temperature Coefficient Resistors Substituted in Place of the Normal Probes.	47
24. Comparison between the Variously Configured Thermosonde Flights.	43
25. Transient Response of Thermosonde to "Switched" Radiation in a Laboratory Chamber.	50
26. Response of Thermosonde to "Switched" Radiation in a Laboratory Chamber at Stratospheric Pressures.	51
27. Measured Air and Electronic Package Temperatures of the Thermosonde.	53
28. Measured Output Voltages as a Function of Calibrated Input $C_T \times R_0$ and Temperature in a Laboratory Chamber.	54

Illustrations

A1. Dependence of ΔT on Altitude and Solar Angle.	62
A2. ΔT vs Altitude for Black, White, and Stainless Steel Probes, for LOWTRAN absorption and for constant absorption.	63
A3. Baseline Shifts – ΔT for LOWTRAN and Constant Absorption.	64

Tables

1. Constants for Determination of Nusselt Number	6
2. Values of Constants and Units	6
3. Emissivities and Absorptivities at Solar Temperature	6
4. Cross Flow Convective Heat Transfer Coefficient	7
5. Values of ΔT for Cross-Flow and Normal Incidence Radiation	7
6. Parallel-Flow Convective Transfer Coefficient	9
7. Cross-Flow and Parallel-Flow Nusselt Numbers	9
8. Days from Winter Solstice	11
9. Estimates of ΔT for Bedford Flight	12
10. Experimental Measurement of ΔT for Bedford Flight	12
11. Baseline Shift Observations (BLS)	19
12. Estimation of ΔT , S/N 6477, Stainless Probes	23
13. Estimation of ΔT , S/N 6469, Stainless Probes	23
14. Estimation of ΔT , S/N 6474, Stainless Probes	23
15. Estimation of ΔT , S/N 5306, Stainless Probes	24
16. Regression $\langle C_T^2 \rangle$ vs. ΔT for Unpainted Stainless Probes	24

Tables

17. Estimation of ΔT , S/N 6485, White Painted Probes	25
18. Regression $\langle C_T^2 \rangle$ vs. ΔT for White Painted Probes	25
19. Regression of All Cases, Table 16 combined with Table 18	26
20. Cold Probe Series, Estimation of ΔT , White Painted Probes	27
21. Regression $\langle C_T^2 \rangle$ vs. ΔT for Cold (White Painted) Probes	28
22. Estimation of Differences between RMS Air Temperature Fluctuations and RMS Wire Temperature Fluctuations by Simulation of Temperature and Velocity Fluctuations by Random Numbers and Consideration of Wire Temperature Distribution	33
23. Specially Configured Thermosondes— Effect on the Isoplanatic Angle, θ_0	49

Study of Possible Solar Heating Effects on Thermosonde Probes — Error Analysis

1. INTRODUCTION

We have observed a diurnal effect in our $\langle C_n^2 \rangle$ measurements in the 15-30 km altitude range. Daytime $\langle C_n^2 \rangle$ values displayed a base line shift (BLS), that is to say, a baseline departure from the noise limit. The effect was that the average C_n^2 values (denoted by $\langle C_n^2 \rangle$) were larger in the daytime. One explanation is that this is due to a real but unknown atmospheric heating effect. But two things tend to oppose the ready acceptance of such an interpretation. The first is that the thermosonde measures "nighttime" values of $\langle C_n^2 \rangle$ within about twenty minutes after sunset. Such a short time seems to be inconsistent with an atmospheric effect. The second is that an alternative explanation with some credibility exists, namely that the diurnal effects are due to solar heating of the thermosonde sensor. This alternative explanation will be investigated in what follows.

Our approach will draw upon experimental measurements from field campaigns and from specially designed balloon flights and laboratory measurements. Theoretical calculations will be compared to the measurements. Figure 1 shows a diagram of the sensor. The thin wire probe between the two stays is used to measure the temperature fluctuations. The stays protrude and are enclosed by the probe support, having a temperature, T_p . In particular we will focus upon the average difference between T_p and the temperature of the immediate environment, T_e , which we call ΔT ($\Delta T \equiv T_p - T_e$). We will make theoretical estimates of ΔT based on heat transfer theory and compare with experimental measurements of ΔT . The probe support, (PS) having temperature T_p ,

(Received for Publication 6 July 1989)

THERMOSONDE PROBE

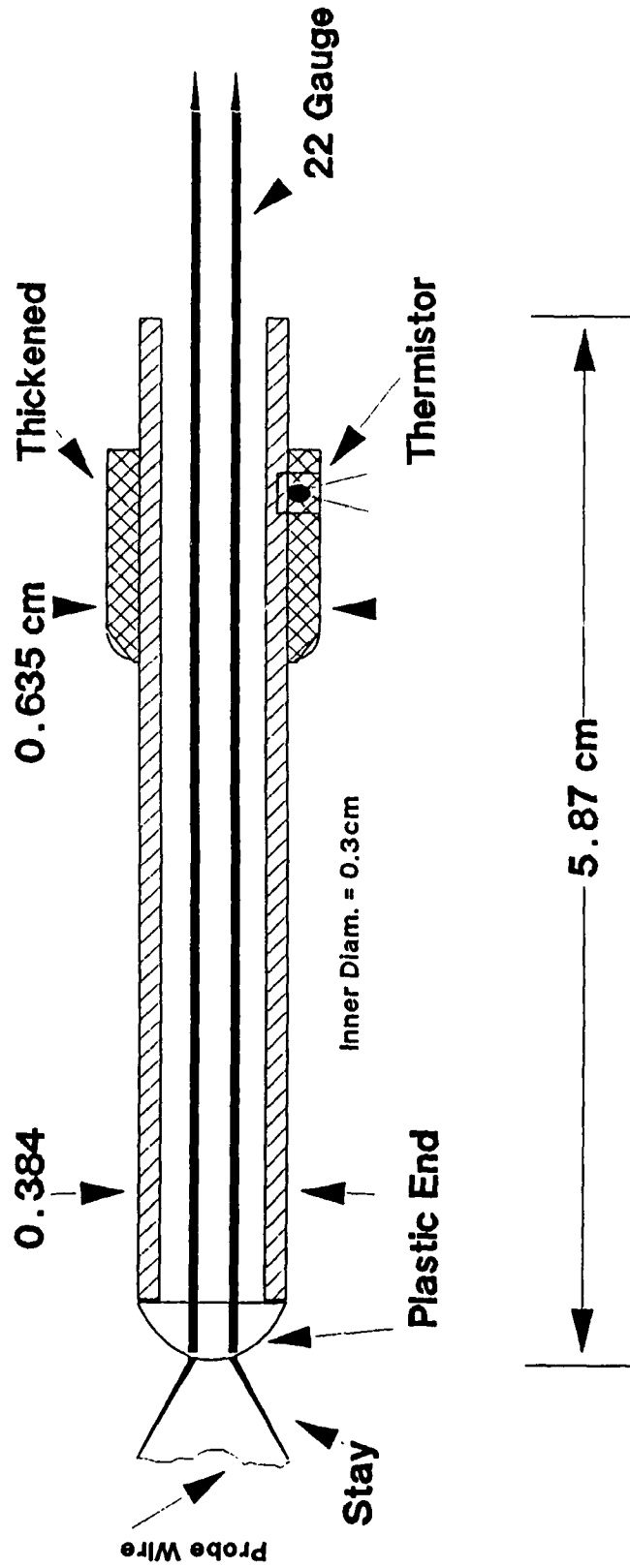


Figure 1. Thermosonde Probe, Diagram.

will be considered as colored white; black; and, in a third case, the stainless steel will be bare (designated SST). As our calculations show, ΔT will depend crucially upon the incident angle, Θ , of the solar radiation, and hence upon launch time, latitude, and season.

Our hypothesis that ΔT can affect $\langle C_n^2 \rangle$ measurements will be tested by comparing $\langle C_n^2 \rangle$ that is, spatially averaged measurements of C_n^2 , with calculated values of ΔT . As will be seen, the statistical evidence supports the artifact (that is, solar heating) hypothesis; however, laboratory measurements and heat transfer considerations do not. There remain several crucial questions that are unanswered and more work must be done before the issue can be settled. For example, we have, as yet, only preliminary atmospheric quantitative models that explain how $\langle C_n^2 \rangle$ or the BLS can be enhanced naturally. We are continuing to explore the possibility that perturbed fine structure ozone layering can produce the necessary gradients in the potential temperature profile to induce instabilities sufficient to cause overturning and turbulence. In a latter section we will discuss a method by which solar radiation and mechanical turbulence could possibly enhance ΔT .

2. HEAT TRANSFER CONSIDERATIONS

2.1 Cross-Flow Convective Transfer in the Presence of Radiative Heat Transfer

In the following $\Delta T \equiv T_p - T_e$ will be calculated from conservation of energy flux. The calculation will involve both direct and indirect solar radiative heating, radiative cooling of the probe and convective cooling in the 15-30 km altitude region. In these calculations we will be concerned exclusively with the PS (probe support) temperature, T_p , and the difference ΔT . We will not consider explicitly, for example, the temperature of the stays, or the temperature of the probe wire. The distribution of temperature along the wire and effects due to small changes velocity will be discussed in a later section. The PS (see Figure 1), is only approximately cylindrical (note the widened middle section). We shall assume for purposes here that sufficient accuracy will result from considering it as a plain circular cylinder of diameter $D = 4 \times 10^{-3}$ m. As will be seen, we have some experimental data to support this assumption.

The conservation of energy-flux equation is given by:

$$\begin{aligned}
 & E_{DS} + E_{RS} + E_{LE} \\
 & \text{(direct solar)} \quad \left(\begin{array}{l} \text{indirect solar:} \\ \text{from atm. reflection} \end{array} \right) \quad \text{(earth radiation)} \\
 & \\
 & = E_{LW} + E_C \\
 & \left(\begin{array}{l} \text{energy radiated} \\ \text{out from PS} \end{array} \right) \quad \text{(energy convected out)}
 \end{aligned} \tag{1}$$

The treatment presented by Brown and Good^{1,2} is followed here.

¹Brown, J.H., Good, R.E., Bench, P.M., Faucher, G., *Sonde Experiments for Comparative Measurements of Optical Turbulence*, AFGL-TR-82-0079, 24 February 1982. ADA118740

²Brown, J.H., and Good, R.E., *Thermosonde and UHF Radar Measurements of C_n^2 at Westford, Massachusetts (Appendix)* - July 1981, AFGL-TR-84-0109, 23 February 1981. ADA145398

$$E_D \equiv \frac{fS\epsilon_T A}{F_D} \text{ (direct solar input)} \quad (2)$$

Where S is the solar flux outside the atmosphere ($\approx 1400 \text{ W/m}^2$), f is the fraction transmitted to the PS, and at 30 km it is estimated² that $f = 0.9$. In our calculations here we will hold fixed to this value but in reality it would depend on time of day (especially near dawn and dusk which won't hurt our calculations for times around noon) and it will also depend a small amount on altitude. F_D is a form factor $= \pi$, A is the PS surface area, and ϵ_T is the solar absorptivity.

$$E_{RS} \equiv \frac{fS\epsilon_T \alpha A}{F_R} \text{ (atmospheric reflection)} \quad (3)$$

Where F_R is the form factor $(=2.0)^2$ and α is the factor for atmospheric scattering ($\alpha = 0.35$ will be used²).

$$E_{LE} \equiv \frac{S_e \epsilon_{LW} A}{F_R} \text{ (long wave radiation from the earth)} \quad (4)$$

Where ϵ_{LW} is the emissivity at long wavelength, (Ref. 3), at the probe temperature or the earth's surface temperature; S_e is the radiated flux from the earth which is³ around 220 W/m^2 at 30 km.

$$E_{LW} \equiv \epsilon_{LW} A \sigma T_p^4 \text{ (long wave radiation from the probe)} \quad (5)$$

Where T_p is the probe support temperature ($^{\circ}\text{K}$) and σ is the Stephan-Boltzman constant $= 5.67 \times 10^{-8} (\text{W/m}^2)/^{\circ}\text{K}^4$. Finally, the convective term is:

$$E_C \equiv hA\Delta T \quad (6)$$

Where $\Delta T \equiv T_p - T_e$ and h is the convective heat transfer coefficient ($\text{W/m}^2\text{K}$). Equations (2)-(6) can be inserted into Eq. (1) and solved for ΔT . For simplicity we assume $\Delta T \ll T_e$, that is, replace T_p^4 in Eq. (5) with T_e^4 , and obtain:

³Morrissey, J. (1972) Atmospheric Temperature Measurements Using Balloons and Rockets. *Temperature Measurements, Geophysical and Astrophysical Temperature Measurements*, Instrument Society of America, **209**: 2299-2311.

$$\Delta T = \frac{1}{h} \left\{ \epsilon_T [401 + 630\alpha] + \epsilon_{LW} (110 - \sigma T_e^4) \right\} \quad (7)$$

(term in square brackets = 621.5 for a = 0.35)

The approximation would incur an error of 60 percent if ΔT were as large as 32° , but 32° is much larger than those values used in this report.

The next topic is the calculation of h . Essentially all textbooks on heat transfer describe how to calculate h for a cylinder immersed in a flow moving across or perpendicular to its axis. This does not apply to our case since the PS moves upward along its axis (that is, we have parallel rather than cross flow). Nevertheless, for reasons that will become clear we will first treat the well-known cross-flow case.

The standard approach^{4,5} starts with the dimensionless Nusselt number, Nu , defined by:

$$Nu \equiv \frac{hD}{k} \quad (8)$$

Where D is the cylinder diameter, k is the conductivity of the fluid (air in our case), and Nu is obtained from:

$$Nu = A(Re)^B \quad (9)$$

Where Re is the Reynold's number, (UD/ν) , U is the ascent velocity of the balloon (≈ 5 m/s), and ν is the kinematic viscosity of the air. The constants A and B in Eq. (9) are listed in Table 1 from Sucec⁶ and attributed to Hilpert⁷. Tables 2 and 3 would then be used with values of h to obtain ΔT from Eq. (7). Table 4 give the values of h calculated in the above manner at selected altitudes. Note that the values of ν and k were obtained from the U.S. Standard Atmosphere of 1976⁸ whereas T_e values were those actually measured in an experiment described below. The latter experiment actually measured PS temperatures and provided ΔT values to compare with theory. Table 5 lists the resulting values of ΔT that were calculated for the three colors (using Table 3). These values, however, suffer from two incorrect assumptions: (a) cross-flow rather than parallel flow was used, and furthermore, (b) the solar radiation incidence angle was assumed to be normal to the cylinder axis, a situation which rarely holds. We will now correct the calculation by considering (a) and (b) below.

⁴McAdams, W. (1942) *Heat Transfer*, McGraw-Hill, 2nd ed., 1942.

⁵Jakob, M. (1949) *Heat Transfer*, John Wiley and Sons, Inc., 1949.

⁶Sucec, J. (1975) *Heat Transfer*, Simon and Schuster (Tech Outlines), 1975.

⁷Hilpert, R. (1933) *Forsch. Geb. Ingenieurw.*, 4:215-224, 1933

⁸NOAA, NASA, and USAF (1976) *U.S. Standard Atmosphere, 1976*, U.S. GPO, Washington, D.C.

Table 1. Constants for Determination of Nusselt Number, Nu^a

Re	A	B	
1-4	0.891	0.330	
4-40	0.821	0.385	Nu = (Re) ^B
40-4000	0.615	0.466	

^aSucec, J., *Heat Transfer*, Simon and Schuster, p 431, 1975.

Table 2. Values of Constants and Units

D = 4 × 10 ⁻³	(m)
S = 1.4 × 10 ³	(W/m ²)
h = units	(W/m ² °K)
σ = 5.67 × 10 ⁻⁸	(W/m ² °K ⁴)
S _e = 220*	(W/m ²) at 30 km
α = 0.35	

* Taken as constant over 15-30 km altitude region of stratosphere.

Table 3. Emissivities (ε_{LW}) at T_e, and Absorptivities (ε_T) at Solar Temperature. Values are approximate. (Sources differed from 15% to 200%)

ABSORPTIVITY ε _T	EMISSIVITY ε _{LW}	COLOR
0.80 ^b	0.80 ^c	Black Paint
0.25 ^d	0.80 ^e	White Paint
0.30 ^f	0.20 ^g	Stainless Steel

^bWolfe, W., and Zissis, G., *The Infrared Handbook*, ONR, Washington D.C., 1978.

^cPitts, D.R., and Sisscom, L.E., *Heat Transfer*, 1977.

^d*Handbook of Chemistry and Physics*, CRC, 35th ed., 1953.

^eMcAdams, W., *Heat Transfer*, McGraw-Hill, 2nd ed., 1942.

^fKoelle, H.H., *Handbook of Astronautical Engineering*, McGraw-Hill, 1961

^gibid.

Table 4. Cross Flow Convective Heat Transfer Coefficient, h.

Alt (km)	$v^*(m^2/s)$	$k^*(W/m^2K)$	Re^\dagger	Nu_{\perp}	$h(W/m^2K)$
15	7.3×10^{-5}	1.95×10^{-5}	274.	8.41	41.0
20	1.6×10^{-4}	1.95×10^{-2}	125.	5.83	28.4
25	3.6×10^{-4}	1.99×10^{-2}	55.4	3.99	19.9
30	8.0×10^{-4}	2.00×10^{-2}	25.0	2.83	14.2

*US Standard Atmosphere 1976.

† $D = 4.0 \times 10^{-3}$ (m)

$U = 5.0$ (m/s)

Table 5. Values of "ΔT" for Cross-Flow and Normal Incidence Radiation

Alt (km)	$T_c^*(^{\circ}K)$	$h(W/m^2K)$	$\Delta T (^{\circ}K)$		
			Black	White	Stainless
15	216	41.0	11.90	3.53	4.48
20	217	28.4	17.10	5.05	6.46
25	225	19.9	23.60	6.39	9.07
30	235	14.2	31.50	7.40	12.2

*Experimental values from Bedford flight.

2.2 Parallel-flow convective transfer for a cylinder

We commence with the general case of arbitrary flow angle (Figure 2) and then proceed to the special case of parallel flow. In Figure 2, the angle χ is the angle between the direction of flow and the coplanar normal to the axis. The effective cooling velocity, U_{eff} is given by:⁹

$$U_{eff} = U(\cos^2 \chi + k^2 \sin^2 \chi)^{\frac{1}{2}} \quad (10)$$

Where U is the flow velocity (in our case 5 m/s). Thus for flow at an arbitrary angle one calculates Re_c on the basis of U_{eff} in place of U and then proceeds to calculate Nu and h as described previously. Equation (10) is based on experiments. It is limited to the range $25^{\circ} < \chi < 60^{\circ}$ and this limitation is due to disruption of the flow caused by the structures holding the ends of the wire. The value of k has been shown experimentally to vary in approximately

⁹Champaign, F., Sleicher, C., and Wehrmann, O. (1967) *J. Fluid Mech.*, **28**:153-175.

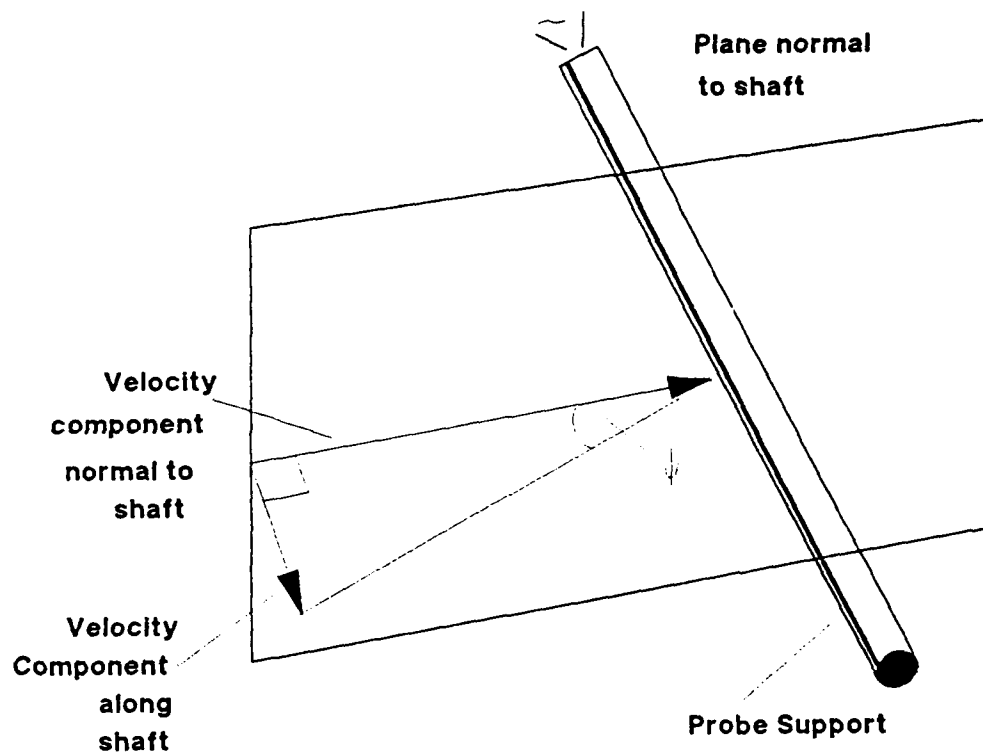


Figure 2. Perspective Drawing, Thermosonde Probe Support and Velocity Vector.

linear fashion with the quantity ℓ/D , where D = diameter and ℓ = length of the wire. At $\ell/D = 200$, $k = 0.20$, and at $\ell/D = 600$ it falls to zero. A straight line fit between these two points gives:

$$k = 0.3 - 5 \times 10^{-4}(\ell/D) \quad (11)$$

This is to be compared with the results of Bullock and Bremhorst who obtained¹⁰

$$k = 0.29 - 4.5 \times 10^{-4}(\ell/D) \quad \text{for } (200 < \ell/D < 600) \quad (12)$$

which is in complete agreement with Eq. (11). Incidentally, a review article¹¹ on this subject, while extremely useful, gives Eq. (12) with the wrong constant (see footnote). For parallel flow,

¹⁰Bullock, K., and Bremhorst, K. (1969) IEEE Transactions on Instruments and Measurements, **IM-18**: 163-166, 1969.

¹¹Morgan, V., The Overall Convective Heat Transfer from Smooth Circular Cylinders. *Advances in Heat Transfer*, **11**, Irvine, T., and Hartnett, J., 1975. Bullock, et. al., 1969, were misquoted and the number, 4.5×10^{-3} was given in place of 4.5×10^{-4} .

then, we extrapolate Eq. (11) to $\chi = 90^\circ$ and $l/D = 15.4$ (for the PS) and obtain:

$$U_{\text{eff}} = kU = 0.292U \quad (13)$$

with $U = 5$ m/s, U_{eff} becomes 1.45 m/s and we arrive at Table 6 for the parallel flow case.

Table 6. Parallel-Flow Convective Transfer Coefficient, $h(\text{W}/\text{m}^2\text{K})$

Alt (km)	Re*	Nu	h
15	76.2	4.63	23.7
20	34.8	3.22	15.5
25	15.4	2.35	12.3
30	6.94	1.73	9.26

$$*D = 3.81 \times 10^{-3} \text{ m}$$

$$U_{\text{eff}} = (0.292)(5 \text{ m/s}) = 1.46 \text{ m/s}$$

Since the above does involve an extrapolation that is a factor of 13 beyond the fitted region, it is desirable to have an independent check upon our results. Fortunately Jakob¹² provides this check. In his work, he gives evidence that in parallel flow the Nusselt number is lowered from its cross-flow value by 40 percent. In other words, the Nusselt number for parallel flow, $Nu ||$, is equal to 60 percent of the Nusselt number for cross-flow, Nu_{\perp} .

Table 7. Cross-Flow and Parallel Flow Nusselt Numbers

Alt (km)	$Nu_{\perp} \times (0.6)$	$Nu $ (Table 6)
15	5.05	4.63
20	3.50	3.22
25	2.39	2.35
30	1.70	1.73

Our independent results can now be compared for verification. Table 7 gives both $Nu ||$ from Table 6 and $(0.60)Nu_{\perp}$ based on Table 4. As can be seen, the agreement is excellent. Henceforth, the values of h listed in Table 6 will be employed.

¹²Jakob, M. (1949) *Heat Transfer*, Vol. 1, p559, fig. 26-4, John Wiley and Sons, 1949.

2.3 Effects Due to Solar Radiation Incidence Angle

The angle formed between the direction of the incident solar radiation and the coplanar normal to the cylinder axis, Θ , will greatly influence the amount of radiant energy absorbed by the probe support. It is well known that if S represents the flux of a beam, the amount of flux (power per unit area) received by a plane surface is given by $S \cos \Theta$ (the "cosine law"). We account for this by replacing S in Eq. (2) with $S \cos \Theta$. For convenience we shall also do this in Eq. (3) and hence throughout Eq. (7) (that is, both terms in the square bracket, (621.5), will be multiplied by $\cos \Theta$). This last step is subject to modification since the actual dependence of atmospheric reflection, Eq. (3), upon Θ is not known to us at this time. For the present purposes this procedure seems to be innocuous in regard to the conclusions that will be reached here; but in future work it may be important to bear in mind that this particular step needs closer examination. In other words, certain conditions may exist to render the model inaccurate. The omission here of Θ dependence upon atmospheric transmission of solar radiation is also to be noted in this context.

Equation (7) thus becomes:

$$\Delta T = \frac{\{\epsilon_T(621.5)\cos\Theta + \epsilon_{LW}(110 - \sigma T_c^4)\}}{h} \quad (14)$$

The value of Θ is, on average, the sun's altitude angle or the angle of the sun above the local horizon. In reality, the pendulum motion of the instrument package will modulate Θ ; however, we will assume in our model that the probe support axis is vertical at all times. The angle Θ is a function of time of day, latitude, and time of year. It is well known from spherical geometry¹³ that:

$$\cos z = \sin \phi \sin d + \cos \phi \cos d \cos t \quad (15)$$

Where z is the solar zenith angle, ϕ the latitude, d the solar declination on the date in question, and t is the "hour angle" from "noon" obtained by multiplying the difference in hours from "standard time noon" by 15° . (This particular procedure gives no more than a 9 percent error at the experiment location). Due to the fact that $z \equiv (90^\circ - \phi)$ we have from Eq. (15):

$$\Theta = \arcsin\{\sin \phi \sin d + \cos \phi \cos d \cos t\} \quad (16)$$

To obtain d , we shall use¹⁴:

$$d = (-23.27) \cos\left(D_{ws} \frac{360.}{365.24}\right) \quad (17)$$

¹³Smart, W. (1960) *Textbook on Spherical Astronomy*, Cambridge Univ. Press, 4th ed.

¹⁴Slocum, J. (1980) *Celestial Navigation with a Pocket Calculator*, Basic Science Press.

where D_{ws} is the number of days from the Winter Solstice, Dec 22, obtained from Table 8.

Table 8. Days from Winter Solstice

Month	Maximum in Month	Total Previous
December	9	9
January	31	40
February	28.24	68.24
March	31	99.24
April	30	129.24
May	31	160.24
June	30	190.24
July	31	221.24
August	31	252.24
September	30	282.24
October	31	313.24
November	30	343.24
December	22	

*From J. Slocum, 1980.

3. THEORETICAL AND EXPERIMENTAL VALUES OF ΔT

In order to calculate ΔT by means of Eq. (14) in conjunction with Eq. (16), it is essential to account for time elapsed from the time of launch so that the payload reaches the altitudes under consideration. For this purpose we employ a rise rate $U = 5$ m/s. In actuality it is known that U varies about this value by about 2 m/s, however it suffices for all our calculations to assume this average value. The values of h are taken from Table 6, and Table 3 provides ϵ_T and ϵ_{LW} for the various colors. To test the model we have made an experimental flight in which the temperatures of the probe supports were measured by means of small thermistors (diameter = 2.4 mm)

implanted below the PS surface and located in the thick region near the back end (see Figure 1). This flight was launched at 9:42 AM EST (14:42 UT) on 30 May, 1985 from Bedford Massachusetts ($\phi = 42^\circ\text{N}$). The theoretical and experimental values are presented in Tables 9 and 10 respectively and graphed in Figures 3a and 3b respectively. The agreement for our purposes is very good and tends to validate the model. Nevertheless it is desirable to obtain additional experimental flights under varied conditions with regard to Θ in view of the omissions from the model such as (a) the previously mentioned transmission effects, (b) the previously mentioned effects of altitude and "correct Θ dependence" of atmospheric reflection, (c) the non-cylindrical shape of the probe support, and (d) time lag effects due to heat capacity and conduction within the probe support structure, and so on.

To demonstrate the importance of Θ , Figure 4 is presented. In this figure Θ is set = 90° . Note

Table 9. Estimates of ΔT for Bedford Flight

A- Flight Parameters- May 30, 9:42 AM EST					
Alt (km)	Time EST	$15^\circ \times (\text{Noon} - t)$ hour angle	Θ	$T_e^* \text{K}$	$h(\text{W}/\text{m}^2\text{K})^*$
15	10.54	21.82	62.5	217	23.7
20	10.82	17.66	64.7	217	16.5
25	11.10	13.49	66.6	225	12.3
30	11.38	9.32	68.1	236	9.26

*From Measurements this flight

†From Table 6

Latitude, $\phi = 42^\circ\text{N}$, Solar Declination = 21.5°N .

B - $\Delta T(^{\circ}\text{K})$ Estimates			
Alt (km)	Black	White	Stainless
15	9.18	2.52	3.51
20	12.1	3.25	4.63
25	13.8	2.72	5.45
30	14.4	0.57	6.09

Table 10. Experimental Measurements of ΔT For Bedford Flight

Alt (km)	Black	White	Stainless
15	6.10	1.65	3.75
20	8.00	1.70	4.90
25	8.40	0.60	4.40
30	10.4	0.70	7.80

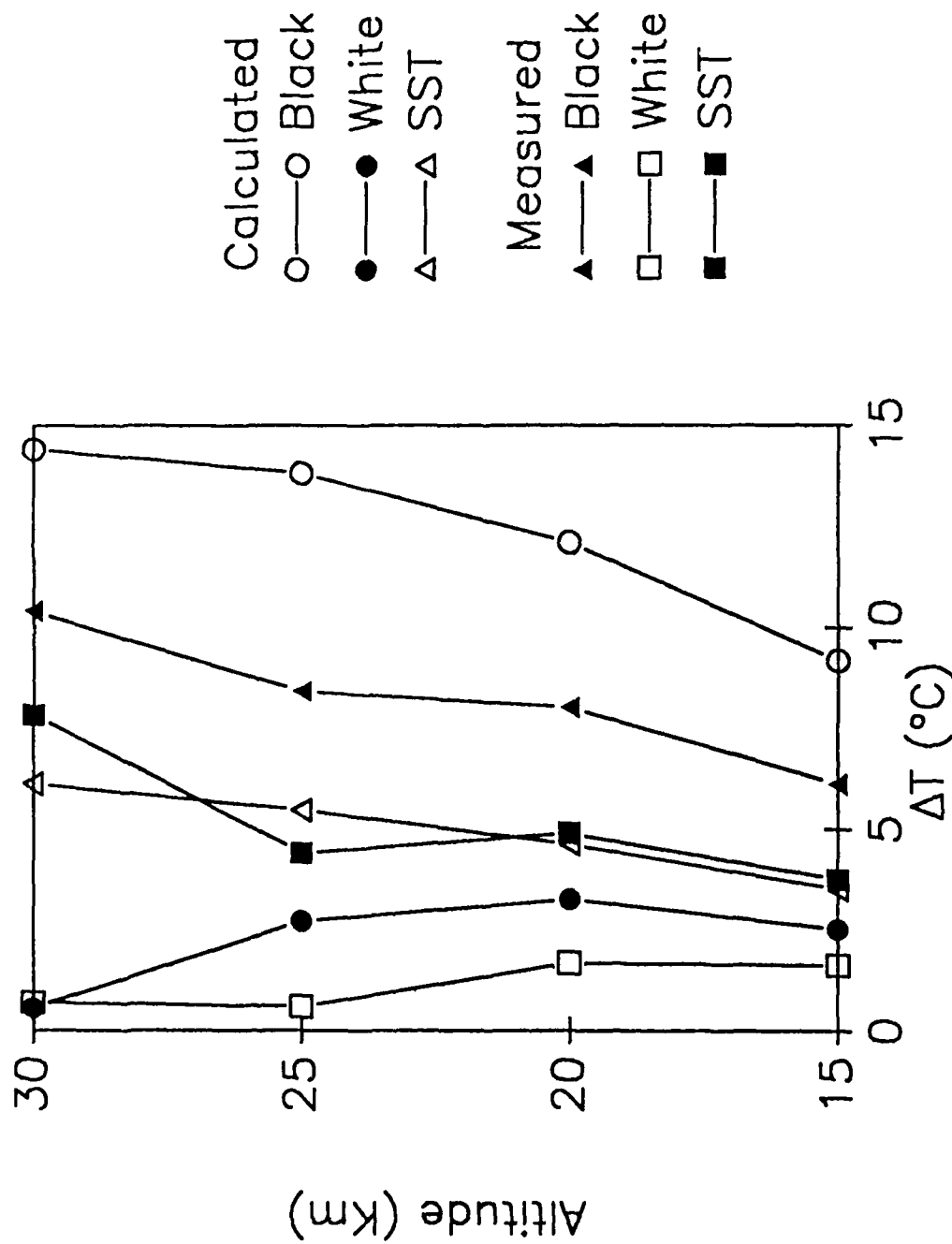


Figure 3, From tables 9B and 10

Figure 3. Increase in Probe Temperature as a Function of Altitude, Calculated and Measured Values for Black, White and Unpainted Probes, from Tables 9B and 10.

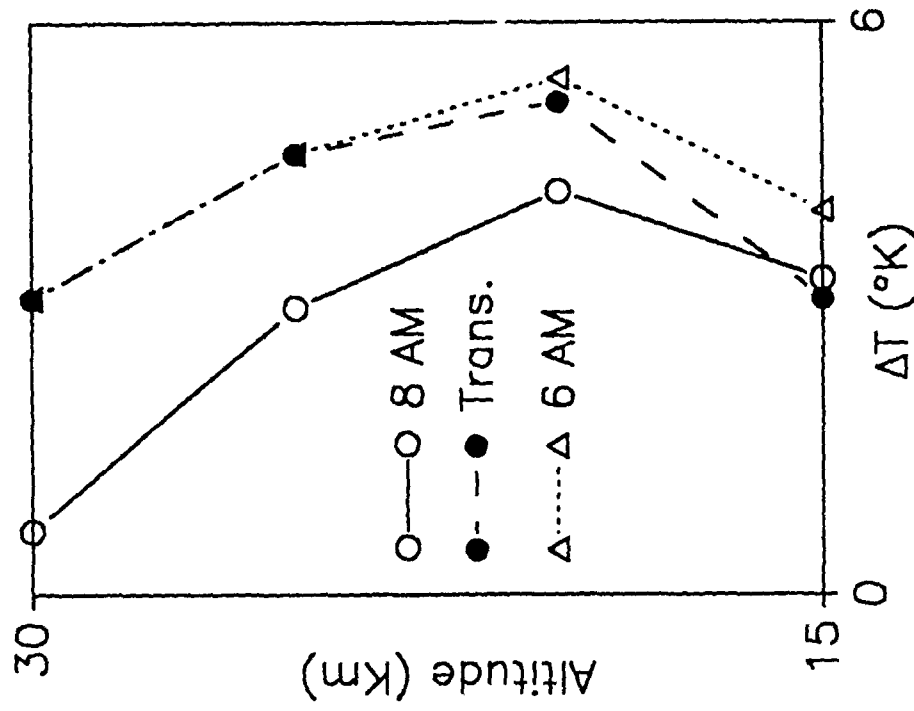


Figure 5. Increase in Probe Temperature as a Function of Altitude. Calculated for 6:00 AM and 8:00 AM.

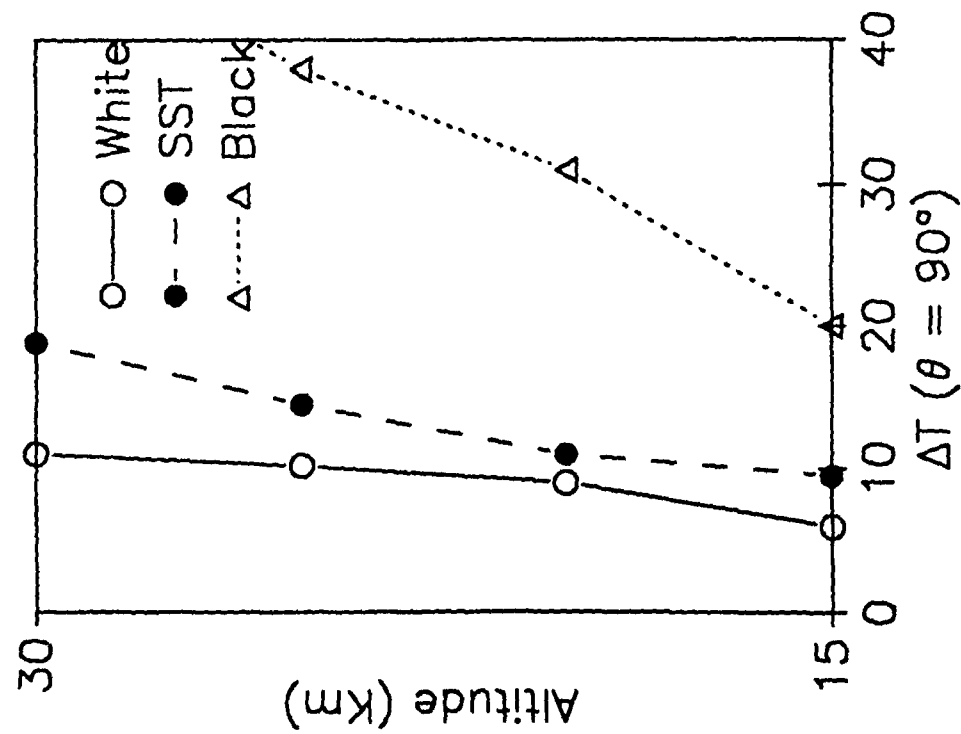


Figure 4. Increase in Probe Temperature as a Function of Altitude. Calculated for a 90° Aspect Angle.

the large differences between ΔT here and the ΔT 's of Figure 3. As can be seen, solar radiation incidence angle is obviously important. To illustrate this fact more realistically, consider Figure 5 for the case of $d = 4^\circ\text{S}$, (that is, -4°), and $\Theta = 21^\circ\text{N}$. In one part of Figure 5 a launch time of 6:25 AM is assumed, whereas, in the other part of the figure it is 8:15 AM. Bear in mind, however, that for small Θ , transmission may play a significant role and that such early flights may, therefore necessitate its inclusion for valid results.

4. EVIDENCE FOR ΔT EFFECTS ON C_T^2 MEASUREMENTS

The purpose of this section is to consider statistical empirical evidence for ΔT effects on $\langle C_T^2 \rangle$. While our main interests are concerned with C_n^2 profiles, it is well known that C_n^2 has a secular decrease with altitude. In contrast, middle stratospheric $\langle C_T^2 \rangle$ profiles do not generally exhibit such a trend. The following relation exists¹⁵ between C_n^2 and C_T^2 .

$$\langle C_T^2 \rangle = \frac{C_n^2}{\left(80 \times 10^{-6} \frac{P}{T^2}\right)^2} \quad (18)$$

Where P is in millibars and T is in $^\circ\text{K}$. The presence of P (associated with the exponential drop of P) with altitude explains why C_n^2 decreases rapidly with increase in height. Thus, to avoid complication we will focus here on $\langle C_T^2 \rangle$ rather than on C_n^2 in the remainder of this discussion.

There are two manifestations of the "diurnal effect" under investigation here, as has been mentioned. The first consists of a shift of the baseline (BLS) of the measurements while the second consists of an enhancement of $\langle C_n^2 \rangle$ and $\langle C_T^2 \rangle$ values in the daytime as compared to nighttime values. The two questions that immediately arise are: (a) "Are these manifestations "real" in the sense that they are not due to artifact?", and (b) "If they are artificial in nature, presumably caused by solar heating related in some way with ΔT , then what is the mechanism by which this takes place?"

At the outset we wish to emphasize that we do not at this time have a validated quantitative model for this mechanism. The question though has been actively investigated. We have postulated that both the BLS and the C_T^2 enhancement may be caused artificially by the non-uniform temperature distribution along the length of wire probe as illustrated in Figure 6. The latter would result from the heat balance between radiation, convection, and conduction to the probe support stays at the ends of the wire. Since the probe support, stays, and wire all have different states of equilibrium, a perturbation in the cooling rate would induce a perturbation in the average wire temperature. If one considers high frequency fluctuations in velocity (C_v^2) and its effect, at stratospheric number densities, on the convective heat transfer coefficient, then by virtue of Eqs. (8) and (9), velocity induced high frequency fluctuations in temperature are conceivable in the wire. A more complete discussion of this possibility will appear later in the report. Now we address the statistical evidence.

¹⁵Tatarski, V.I. (1961) *Wave Propagation in a Turbulent Medium*, McGraw-Hill, 1961.

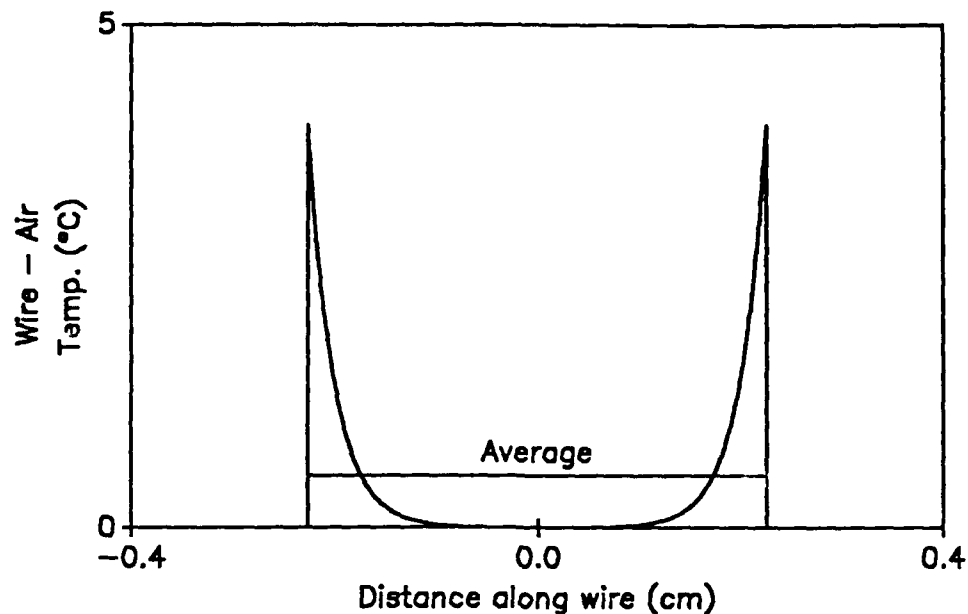


Figure. 6. Distribution of Wire-Air Temperature as Function of Distance along Wire.

4.1 Baseline Shift (BLS)

Figure 7 presents two examples of C_n^2 profiles, one with and one without a BLS. As can be seen, the BLS consists of shifts on C_n^2 values from the noise limited baseline. It is caused either by the condition of the atmosphere (that is, real) or it is artificially induced (from probe heating or changes induced in the electronic sensitivity). Table 11 lists flights along with the presence (YES) or absence (NO) of BLS. The maximum estimated ΔT 's of these flights are also listed.

Two cases show a question mark indicating that a subjective determination cannot be made regarding the presence or absence of a BLS. There are 3 YES cases and 3 NO cases. As can be seen, the highest ΔT indicated in the NO category is 3.6° , whereas the lowest ΔT for the YES category is 5.5° . This separation ($\approx 4^\circ$) is consistent with the hypothesis that the BLS is caused by ΔT . Statistically though, Table 11 does not provide acceptable "significant" evidence for the association of high temperatures with drift (we estimate that, omitting the question marks, the results have an 8 percent probability of being due to chance alone). Added to this is the fact that one case shows a BLS for $\Delta T = 5.5^\circ$, whereas another shows a question mark for $\Delta T = 10^\circ$. The question is: "How can one explain this observation if the BLS is caused by ΔT ?"

M6410
LAUNCH: 02-28-85 01:05:43 UT

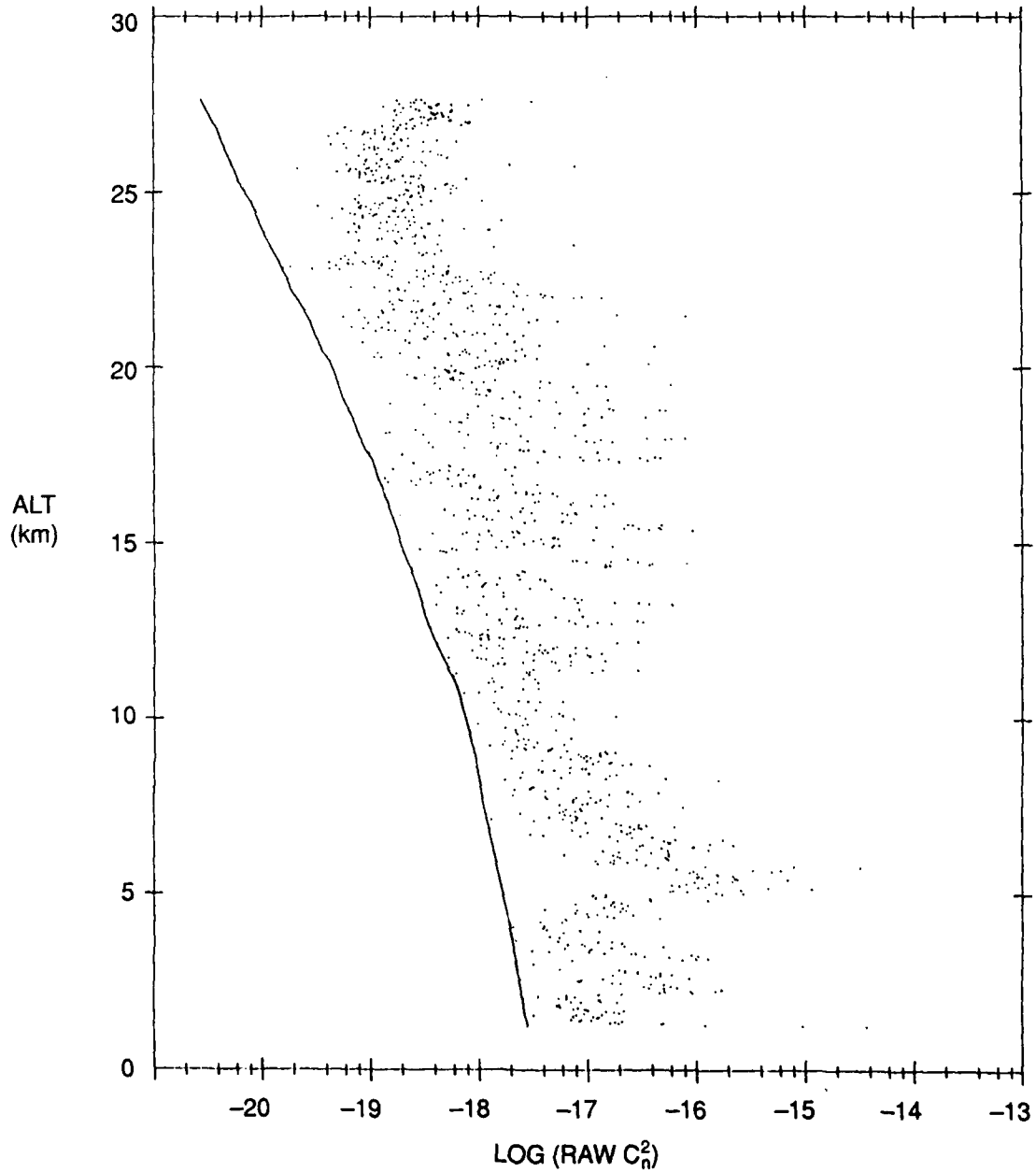


Figure 7a. Thermosonde Measured Values of C_n^2 as a Function of Altitude, Raw Data for Nighttime Profile M6410. Solid line represents instrumental noise limit.

M6388
LAUNCH: 03-04-85 22:22:20 UT

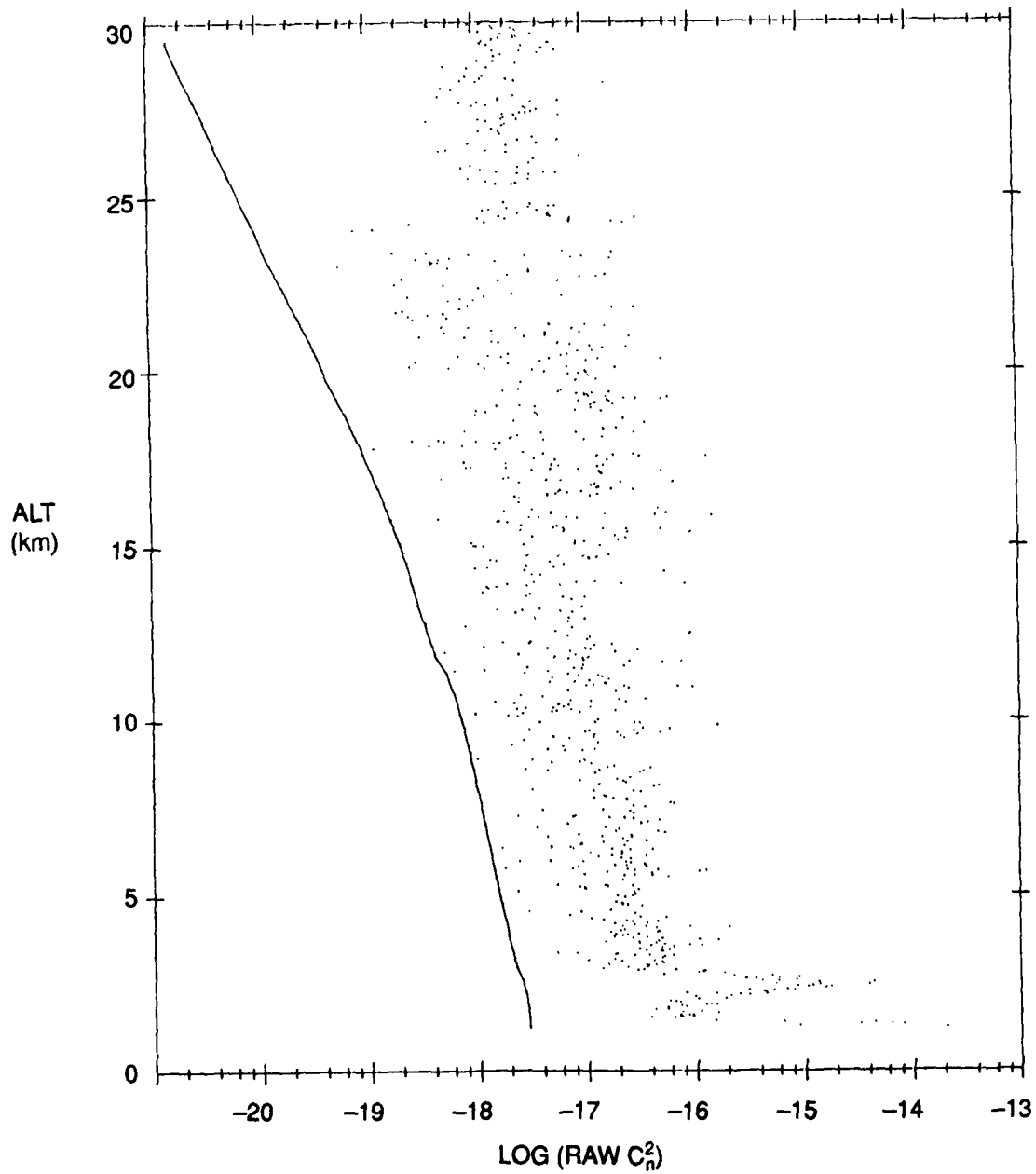


Figure 7b. Thermosonde Measured Values of C_n^2 as a Function of Altitude, Raw Data for Daytime Profile M6388. Solid line represents instrumental noise limit.

Table 11. Baseline Shift Observations (BLS)

Max ΔT	BLS	Launch Time	Probe Color	S/N	
1.70	No	11:21 AM	White	6481	
2.30	?	11:16 AM	White	6466	
2.30	No	11:08 AM	White	6483	
3.60	No	11:06 AM	SST	6477	
5.50	Yes	01:06 PM	White	6485	
9.00	Yes	12:14 PM	SST	6469	
10.00	?	01:44 PM	SST	6474	
13.00	Yes	03:19 PM	SST	5306	Sig. Level = 0.078 (not sig but suggestive)

4.2 Correlation between C_T^2 and ΔT

Figure 8 presents C_T^2 data from one flight as an example. Three forms are given: (a) a Gaussian averaged profile with 40 m half width, (b) a running average (arithmetic) over 300 m, and (c) a block average (arithmetic) over intervals of 2.5 km. In our regression analysis we employ (c) and call it $\langle C_T^2 \rangle$. The $\langle C_T^2 \rangle$ values are regressed against ΔT , and Tables 12-15 contain the estimates of ΔT for all of the unpainted stainless steel PS flights that are being considered. Table 16 couples these ΔT 's with measured C_T^2 's and gives the regression results. The correlation coefficient, γ , has a value of 0.522 from 22 points. To obtain the level of statistical significance (in the form of a percent probability of the correlation being due to chance alone) we make use of the t-statistic relationship¹⁶.

$$t = \frac{\gamma\sqrt{(N-2)}}{\sqrt{(1-\gamma^2)}} \quad (19)$$

Where N is the number of fitted points. In the case at hand, $t = 2.74$ with $N-2 = 20$ degrees of freedom yielding¹⁷ a significance level of less than 2 percent which is considered good statistical evidence.¹⁸

¹⁶Morony, M., (1951) *Facts and Figures*, Penguin Books, Ltd., 1951.

¹⁷Burlington, R., and May, D. (1953) *Handbook of Probability and Statistical Tables*, Handbook Pub., Inc., Ohio, 1953.

¹⁸A regression on the $\cos \Theta$ gave no correlation. This results favors the probe heating rather than the atmospheric heating interpretation.

M6483
LAUNCH: 08-02-85 18:08:08 UT

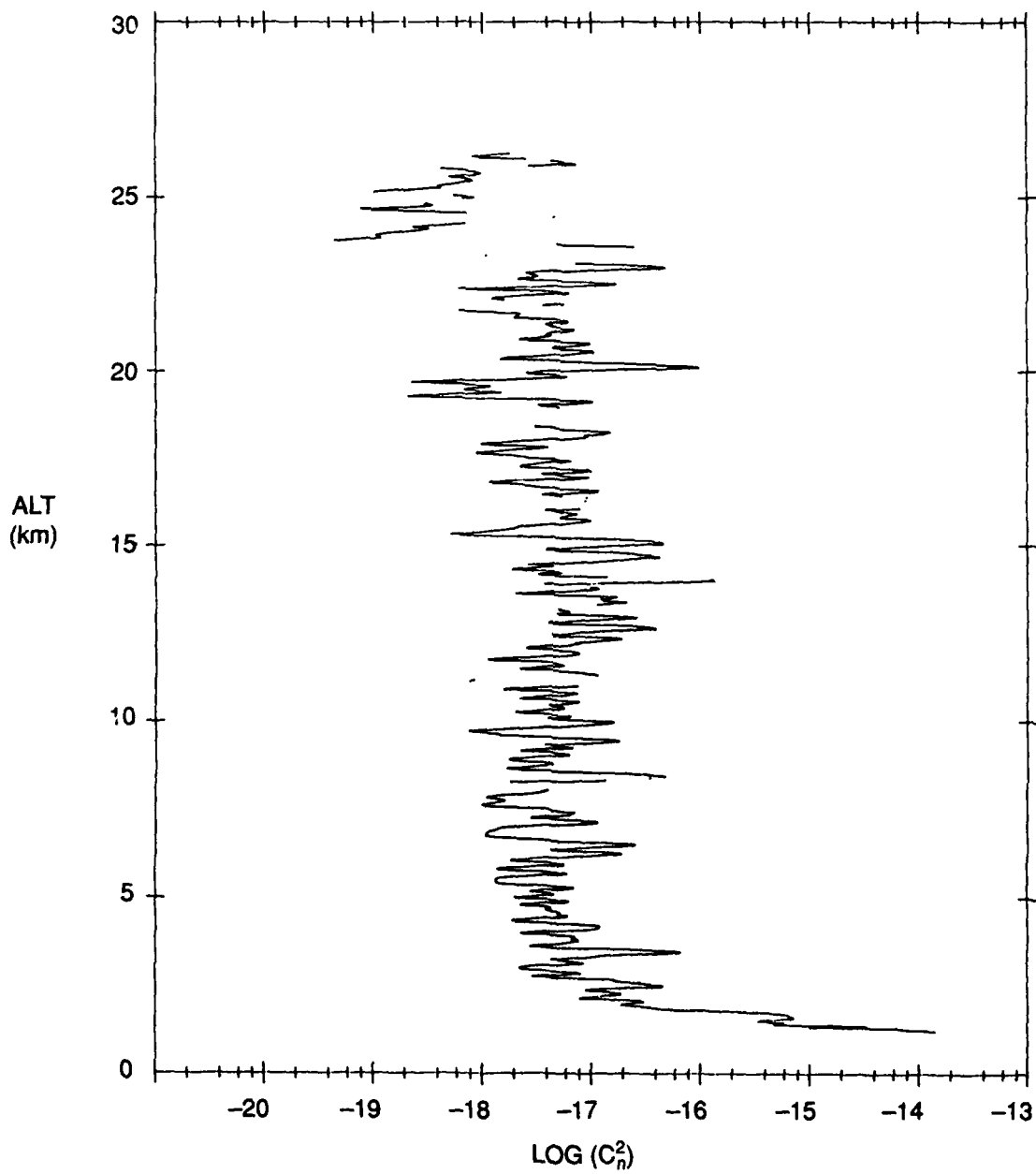


Figure 8a. Gaussian Averaged Profile for Flight M6483, $\sigma = 40$ meters.

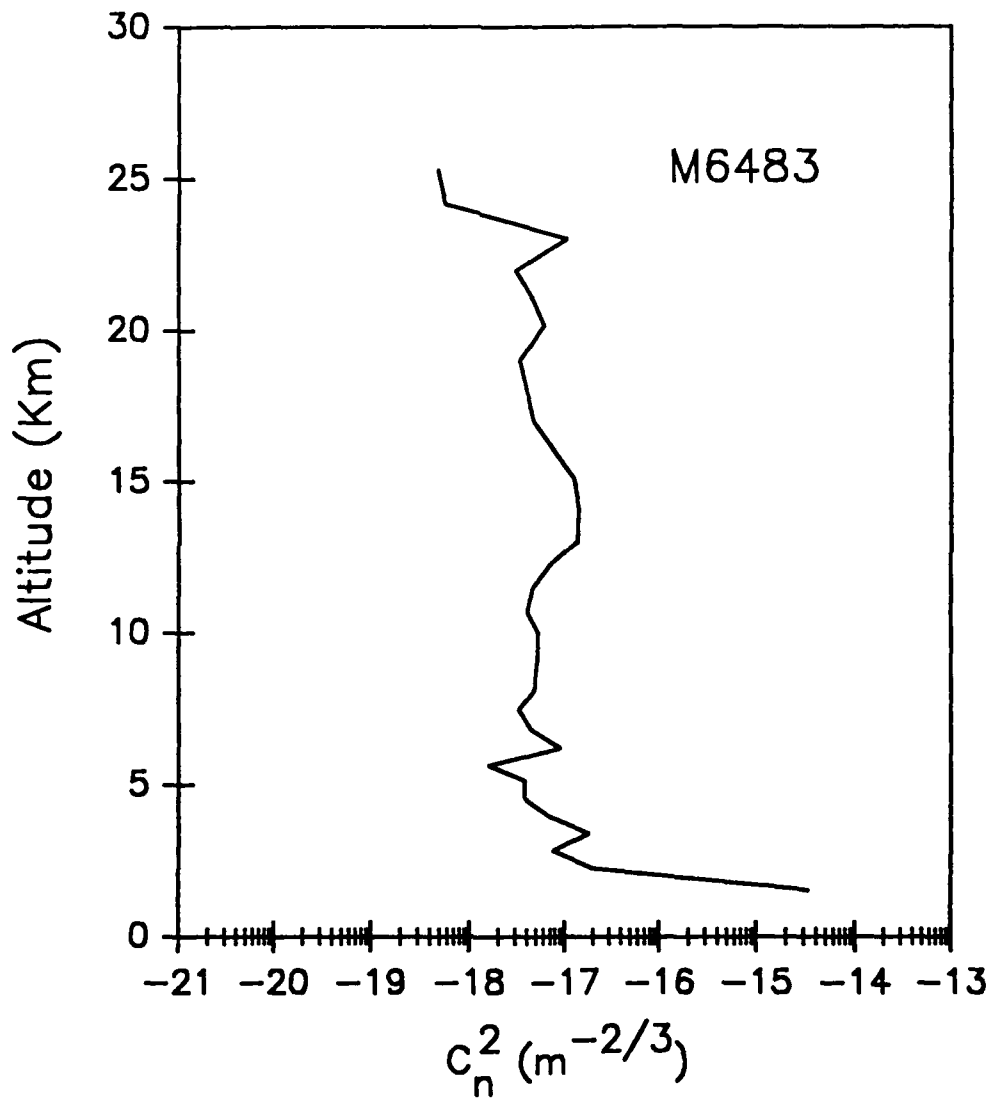


Figure 8b. 500 Meter Running Average Profile for Flight M6483.

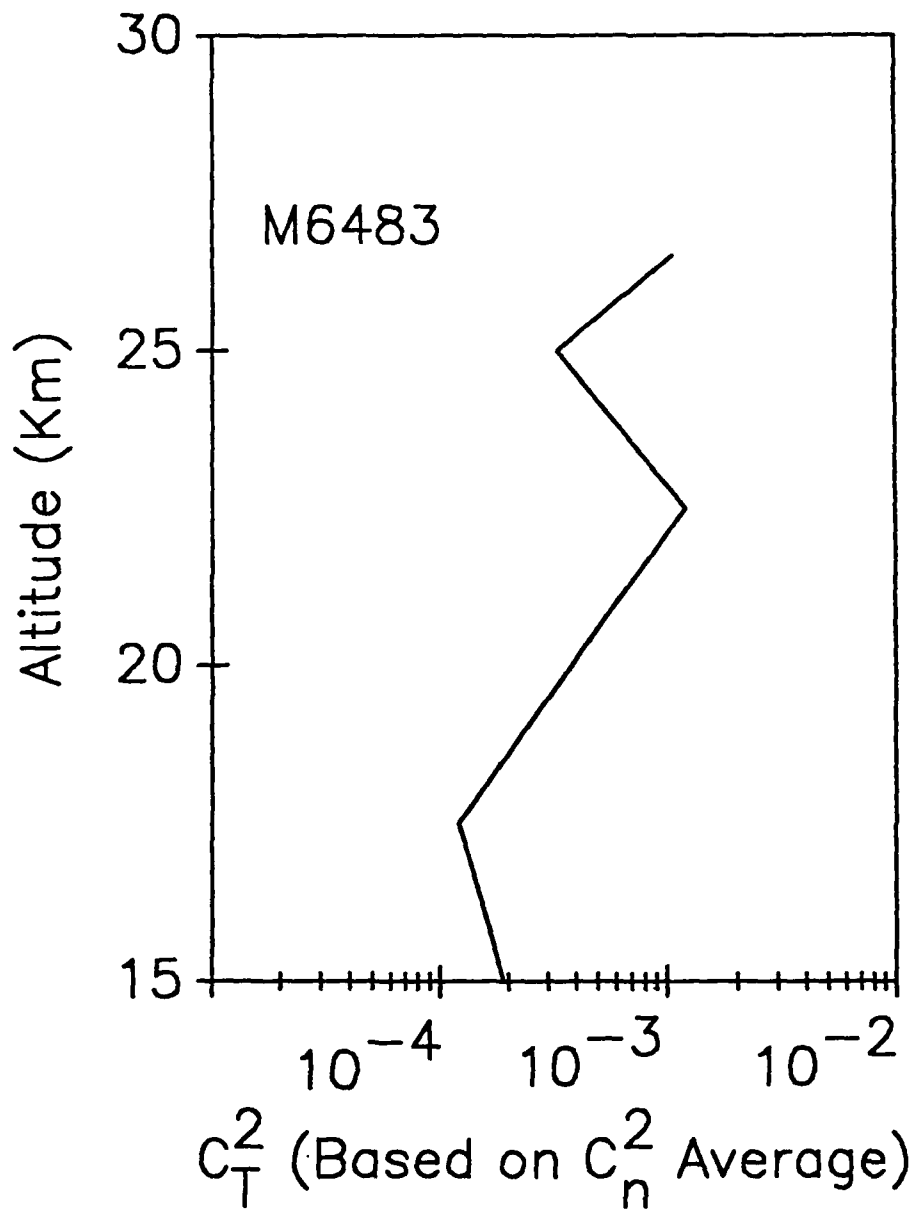


Figure 8c. 2500 Meter Box Average C_T^2 Profile for Flight M6483.

Table 12. Estimation of ΔT , S/N 6477
 11:06 AM, $d = 18^\circ\text{N}$, $\phi = 32.2^\circ\text{N}$, Stainless Steel

Alt (km)	θ°	$h(\text{W}/\text{m}^2\text{K})$	T_e *°K	ΔT °K
15.0	75.8	23.7	217	1.81
17.5	75.8	19.8	217	2.17
20.0	75.5	16.5	217	2.63
22.5	75.0	14.2	219	3.11
25.0	74.3	12.3	223	3.61

*US Standard Atmosphere

Table 13. Estimation of ΔT , S/N 6469
 12:14 PM, $d = 18^\circ\text{N}$, $\phi = 32.2^\circ\text{N}$, Stainless Steel

Alt (km)	θ°	$h(\text{W}/\text{m}^2\text{K})$	T_e *°K	ΔT °K
15.0	69.8	23.7	217	2.59
17.5	68.4	19.8	217	3.13
20.0	67.0	16.5	217	4.23
22.5	65.5	14.2	219	5.16
25.0	63.9	12.3	223	6.17
27.5	62.3	10.7	224	7.49
30.0	60.7	9.26	227	8.97

*US Standard Atmosphere

Table 14. Estimation of ΔT , S/N 6474
 01:44 PM, $d = 18^\circ\text{N}$, $\phi = 32.2^\circ\text{N}$,
 h and T_e as in Table 13,
 Stainless Steel

Alt (km)	θ°	ΔT °K
15.0	52.7	4.64
17.5	50.9	5.78
20.0	49.2	7.19
22.5	47.5	8.59
25.0	45.7	10.1

Table 15. Estimation of ΔT , S/N 5306
 03:32 PM, $d = 18^\circ\text{N}$, $\phi = 32.2^\circ\text{N}$,
 h and T_c as in Table 13,
 Stainless Steel

Alt (km)	θ°	ΔT °K
15.0	32.6	6.50
17.5	30.8	7.78
20.0	29.1	9.68
22.5	27.3	11.4
25.0	25.6	13.2

Table 16. Regression $\langle C_T^2 \rangle$ vs. ΔT for unpainted Stainless Probes
 ($\langle C_T^2 \rangle$ is the arithmetic average over 2.5 km intervals)

Alt (km)	ΔT	$\langle C_T^2 \rangle$ $\times 10^4$	Profile
15.0	1.80	0.72	6477
17.5	2.20	1.60	
20.0	2.60	1.60	
22.5	3.10	3.70	
25.0	3.60	1.50	
15.0	2.60	0.90	6469
17.5	3.30	1.00	
20.0	4.20	2.00	
22.5	5.20	3.30	
25.0	6.20	3.10	
27.5	7.50	18.0	
30.0	9.00	23.0	
15.0	4.60	0.91	6474
17.5	5.80	1.20	
20.0	7.20	1.90	
22.5	8.60	3.70	
25.0	10.1	4.30	
15.0	6.50	0.97	5306
17.5	7.80	3.70	
20.0	9.70	5.10	
22.5	11.0	10.0	
25.0	13.0	7.80	
$N = 22, \langle C_T^2 \rangle \times 10^4 (\text{°K}^2\text{m}^{-2/3}) = -1.28 + 0.945\Delta T$ $t = 2.74, df = 20, r = 0.522$ Significance Level < 0.02 (Significant)			

Next we consider a flight with a white colored probe launched at a time of day such that elevated levels of ΔT are reached. Tables 17 and 18 give ΔT and regression calculations. A correlation coefficient of value $\gamma = 0.942$ is the main result. Using Eq. (19) we obtain $t = 4.86$, three degrees of freedom (not much) but again there is a better than 2 percent level of significance. All the above were combined (see Table 19 and Figure 9 for the regression curve) yielding $\gamma = 0.510$, $t = 2.97$, $df^{19} = 25$, and a significance level of better than 1 percent. Thus the statistical correlation for this data set is established in the sense that it has 1:100 odds of being due to chance effects.

Table 17. Estimation of ΔT , S/N 6485
01:06 PM, $d = 18^\circ N$, $\phi = 32.2^\circ N$,
 h and T_e as in Table 13, White
Painted Probes

Alt (km)	Θ°	ΔT °K
15.0	60.3	2.72
17.5	58.6	3.44
20.0	57.0	4.37
22.5	55.3	5.08
25.0	53.7	5.54

Table 18. Regression (C_T^2) vs. ΔT for White painted Probes
($\langle C_T^2 \rangle$ is the arithmetic average over 2.5 km intervals)

Alt (km)	ΔT	$\langle C_T^2 \rangle$ $\times 10^4$	Profile
15.0	2.72	1.13	6485
17.5	3.44	3.13	
20.0	4.37	3.66	
22.5	5.08	6.95	
25.0	5.54	10.2	
$N = 5, \langle C_T^2 \rangle \times 10^4 (\text{K}^2 \text{m}^{-2/3}) = -7.29 + 2.91 \Delta T$			
$t = 4.86, df = 3, r = 0.942$			
Significance Level < 0.02 (Significant)			

¹⁹(degrees of freedom)

Table 19. Regression of all cases given in previous tables
(Table 16 combined with Table 18)

$\langle C_T^2 \rangle \times 10^4 (\text{°K}^2 \text{m}^{-2/3}) = -0.665 + .913\Delta T$ <p> $t = 2.97, df = 25, r = 0.510$ Significance Level < 0.01 (Good Significance) </p>
--

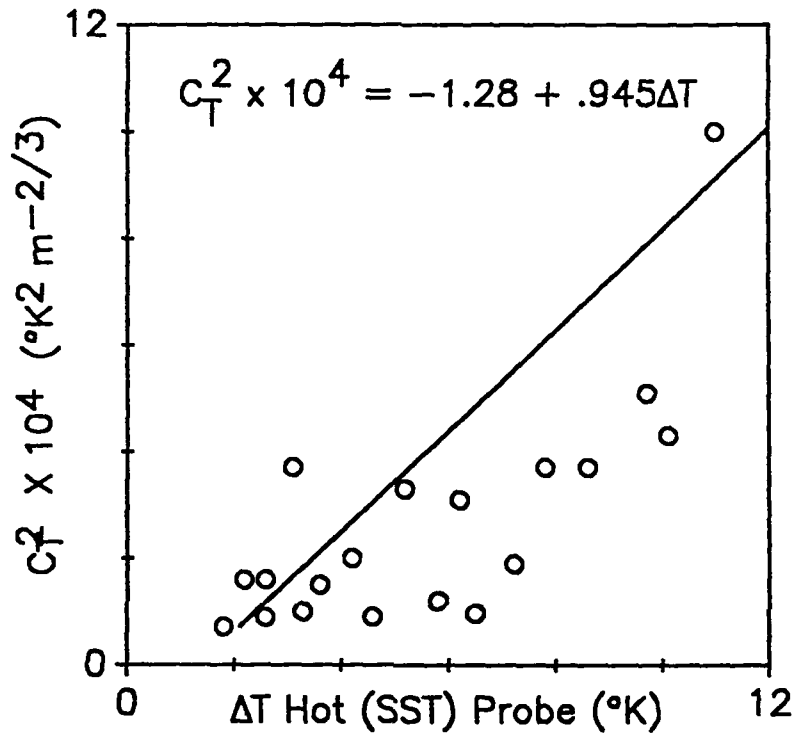


Figure 9, From Table 16

Figure 9. Average Measurements and Regression Curve of C_T^2 as a Function of Calculated Temperature Increase for Unpainted Stainless Steel Probes.

The above results are in marked contrast to the next set of data consisting of three flights, with white painted probes, which were flown at a time of day when ΔT is calculated to have relatively small values. The analysis is summarized in Tables 20 and 21. Figure 10 shows the regression curve (29 points). We obtained $\gamma = 0.162$, $t = 0.68$, $df = 17$, and a significance level of approximately 50 percent. Thus no evidence of correlation exists for this data set. It should be noted that time of day is even more important than the color of the probe in the determination of ΔT . In summary, the statistical correlations between ΔT and $\langle C_T^2 \rangle$ variations and also the lack of them in the last set give consistent statistical evidence for the hypothesis that ΔT and $\langle C_T^2 \rangle$ variations are statistically correlated when ΔT becomes larger than a certain value.

Table 20. Cold Probe Series, Estimation of ΔT
 $d = 18^\circ N$, $\phi = 32.2^\circ N$. Based on launch
time 11:21 AM h and T_e as in Table 13.
White Painted Probes S/N 6481, 11:21
AM; S/N 6466, 11:16 AM

Alt (km)	Θ°	ΔT °K
15.0	75.6	1.10
17.5	75.2	1.40
20.0	74.5	1.70
22.5	73.7	2.30
25.0	72.7	1.80
27.5	71.5	2.20
30.0	70.2	2.10
S/N 6483, 11:06 AM		
Alt (km)	Θ°	ΔT °K
15.0	75.8	1.09
17.5	75.8	1.31
20.0	75.5	1.59
22.5	75.0	1.68
25.0	74.3	1.45

Table 21. Regression $\langle C_T^2 \rangle$ vs. ΔT for Cold (White painted) probes
 ($\langle C_T^2 \rangle$ is the arithmetic average over 2.5 km intervals)

Alt (km)	ΔT	$\langle C_T^2 \rangle$ $\times 10^4$	Profile
15.0	1.10	0.89	6481 (11:21 AM)
17.5	1.40	0.75	
20.0	1.70	1.30	
22.5	2.30	1.00	
25.0	1.80	1.30	
27.5	2.20	1.50	
30.0	2.10	6.30	
15.0	1.10	0.95	6466 (11:16 AM)
17.5	1.40	3.40	
20.0	1.70	1.60	
22.5	2.30	1.80	
25.0	1.80	2.40	
27.5	2.20	2.70	
30.0	2.10	2.30	
15.0	1.10	1.80	6483 (11:08 AM)
17.5	1.30	1.60	
20.0	1.60	5.00	
22.5	1.70	16.0	
25.0	1.50	4.50	
$N = 19, \langle C_T^2 \rangle \times 10^4 (\text{°K}^2 \text{m}^{-2/3}) = 1.98 + 0.60 \Delta T$			
$t = .293, df = 17, r = 0.071$			
$\text{Significance Level} \cong 0.80 \text{ (Not Significant)}$			

4.3 Discussion

Results from these statistics suggest that larger ΔT can cause Baseline Shift (BLS) effects and $\langle C_T^2 \rangle$ enhancement. On the other hand, such causation cannot be proven on the basis of such

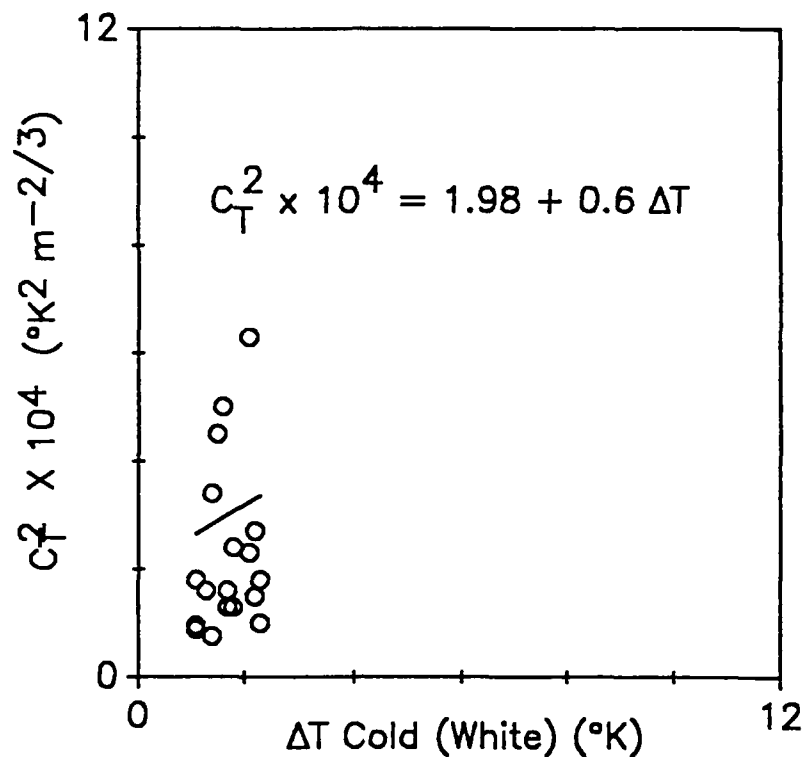


Figure 10, From Table 21

Figure 10. Average Measurements and Regression Curve of C_T^2 as a Function of Calculated Temperature Increase for White Painted Probes.

statistics alone as is well known. For example, take for the case of argument the very hypothetical possibility that there is a real atmospheric phenomenon which causes the BLS and $\langle C_T^2 \rangle$ enhancement in a manner similar to the behavior of ΔT . Our results are consistent with this possibility. In order to establish a cause and effect relationship, other field experiments are necessary, such as, flying longer wire probes and flying more highly reflective probes. Additional low density laboratory simulations of the solar effect will be helpful. These tests and others, in fact, have been performed and they will be described later. It should be noted, however, that both the BLS and $\langle C_T^2 \rangle$ enhancement (regression) observations described above suggest that some ΔT in the region of 4° divides the data into two categories: (a) those which tend to show BLS and high $\langle C_T^2 \rangle$ correlations with ΔT , and (b) those which don't have these tendencies.

In our analysis of how we calculated ΔT , a number of approximations and omissions were mentioned. Most serious, perhaps, especially at smaller values of Θ , was the omission of transmission effects along the path of the solar radiation due to atmospheric absorption, aerosol effects, and scattering. If necessary, these could be incorporated into our model by using LOW-TRAN. On the other hand it is probably more practical to stick with the present procedure of measuring ΔT of the probe support directly during experimental flights. Other theoretical

improvements would result from better estimates of the albedo effects. These were taken into account above in a manner which did not allow for altitude variation, cloud cover effects and varying properties of the earth's surface as a function of season and location. Also there was the problem that was mentioned concerning the $\cos \Theta$ factor in regard to atmospheric reflection.

Finally it should be noted that our calculations of ΔT have omitted time lag effects due to the heat capacity of the probe support. Preliminary calculations show that the time lag factor $\tau = (mC_p/hA)$ (where m is the probe support mass (1×10^{-2} kg), C_p is the specific heat of stainless steel (465 J/kg $^\circ$ K), h is the convective heat coefficient of the support at 30 km (9.26 W/m 2 °K), and A is the surface area (9.42×10^{-4} m 2)). The value of τ is 533 seconds or of the order 10 minutes; therefore, the probe support equilibrium temperature would (for uniform atmospheric temperature gradient and with other factors (net solar input) held constant) lag by an altitude of 3 km at most. This would not affect the conclusions drawn from the calculations of ΔT in this report; however, such effects would be important for nighttime calculations of ΔT which are not considered here.

5. TESTS FOR THE DETERMINATION OF THE REALITY OF THE DIURNAL EFFECTS

To determine if $\langle C_T^2 \rangle$ enhancements and the BLS are due only to real atmospheric changes, the most direct approach would consist of measuring $\langle C_n^2 \rangle$ (or $\langle C_T^2 \rangle$) by two independent methods simultaneously, the first by means of balloon borne thermosondes (the usual manner) and the second by optical instrumentation including isoplanometer, or by radar²⁰. If both measurements showed consistent and dramatic diurnal effects, and if artifact could be ruled out of the second method, then it would seem the phenomenon could be presumed real. Certainly, if the outcome were that the thermosonde sees a large effect, then this would settle the issue in favor of the artifact hypothesis. (Of course unknown effects could prevent the second method seeing the effect, in which case it would be necessary to develop a third technique). In fact, we have conducted simultaneous measurements^{21,22,23,24} of turbulence with thermosondes, radar, and isoplanometer in coordinated programs with Lincoln Laboratory, the Army Atmospheric Sciences Laboratory, and with NOAA. The radar data is mostly low altitude, volume averaged measurements that were not able to reveal a discernible effect. the isoplanometer data did tend

²⁰Nastrom, G., Gage, K., Balsley, B., *Optical Engineering*, **21**:347, 1982. These authors report radar observations of diurnal variations of C_n^2 of 3 to 10 dB in the stratosphere.

²¹Good, R.E., Watkins, B.J., Quesada, A.F., Brown, J.H., and Loriot, G.B., (1982) Radar and Optical Measurements of C_n^2 , *Applied Optics*, **21**:3373-3376.

²²Brown, J.H., and Good, R.E. (1984) *Thermosonde and UHF Radar Measurements of C_n^2 at Westford, Massachusetts*— July 1981, AFGL-TR-84-0109. ADA145398

²³Eaton, F.D., et. al. (1988) Comparisons of VHF Radar, Optical, and Temperature Fluctuation Measurements of C_n^2 , r_0 , and Θ_0 , *Theor. Appl. Climatol.*, **39**:17-29, 1988.

²⁴Warnock, J.M., et. al. (1989) Comparison Among Clear-Air Radar, Thermosonde, and Optical Measurements and Model Estimates of C_n^2 in Very Flat Terrain Over Illinois, Middle Atmospheric Program, *MAP Handbook*, Volume 28, 1989.

to agree with the in-situ thermosonde data when due consideration was given to spatial and temporal path differences. Incontrovertible daytime agreement between the thermosonde calculated values of the isoplanatic angle and the isoplanometer measurements was not always obtained however²⁵. Thus a question mark continues to exist on the daytime stratospheric C_n^2 measurements.

That the diurnal effect may be due to artifact is a very real possibility but it cannot be proven on the basis of the described model nor from the optical/thermosonde comparisons. An important role is played, however, by quantitative models. In the case of the artifact hypothesis, important contributions are made by radiative, convective, and conductive heat transfer as well as probe geometry, thermal boundary layer flow, and dynamic temperature fluctuation. In the case of the atmospheric hypothesis, a prominent role may be played by local heating of high altitude layers of absorbent constituents such as aerosol and thin layers of high ozone concentration. The importance of such models is that they allow testable predictions to be made which then lead to further verification.

5.1 Possible Mechanism for Observed BLS

As alluded to earlier, we have postulated that the BLS and $\langle C_T^2 \rangle$ enhancement might be caused by the combination of effects due to radiative solar heating of the body of the probe, conduction of heat from the PS to the wire, and high frequency fluctuations in the rate of convective cooling. The distribution of temperature along the length of the wire is bounded at the ends by the "hotter" needle supports, and in the center (if optimally engineered) by the ambient temperature. Thus the wire temperature decays asymptotically at the ends from the needle temperature and it asymptotically approaches the ambient temperature near the center. Figure 6 illustrates the distribution. The steady state distribution is expressed as²⁶:

$$\Theta = \frac{\Theta_0 [e^{mx} + e^{-mx} e^{2mL}]}{[1 + e^{2mL}]} \quad (20)$$

Where $\Theta = (t(x) - t_c)$, $\Theta_0 = (t_0 - t_c)$, $t(x)$ is the temperature as a function of the distance, x , along the wire, t_c is the ambient temperature of the environment, and t_0 is the "reservoir" temperature at the ends of the wire (needle supports). L is one half the wire length and $m = \sqrt{(hC/kA)}$, where C is the circumference of the wire ($2\pi r$), A the cross sectional area (πr^2), and h is the convective heat transfer coefficient. In our case (lower stratospheric altitudes) h is approximately $0.048 \text{ Cal}/(\text{cm}^2 \cdot \text{sec} \cdot \text{deg})$, k is approximately $0.426 \text{ Cal}/(\text{cm} \cdot \text{sec} \cdot \text{deg})$, and m is about $25. \text{ cm}^{-1}$. Figure 6 plots this function for $\Theta_0 = 4. \text{ deg}$. Clearly the average wire temperature is influenced by the needle support temperature. The average temperature is calculated by integrating Eq. (20) over

²⁵Eaton, F., et. al. (1989) Comparisons of the Transverse Coherence Length and Isoplanatic Angle Measurements Taken with the Flatlands VHF Radar, Optical Techniques, and Thermosondes, *OE/LASE 89 SPIE Symposium, Proceedings*, April 1989.

²⁶Jakob, M. (1949) *Heat Transfer*, 1, p213, eqs. 11-18, John Wiley and Sons, Inc., 1949.

the wire length. The mean temperature then is:

$$\Theta_{ave} = \frac{2\Theta_0}{mL} \quad (21)$$

which for our case, $\Theta_{ave} = 0.516$ deg.

The thermosonde sensor consists of two wires exposed to the ambient environment and spaced apart by 1 m. If each probe has identical geometry, then there will be no DC (low frequency) difference in the average wire temperatures. Each wire though, will have slightly different geometry (Manufacturing specifications for our probes constrain the resistances to 26.5 ohms \pm 1 ohm at 22°C). For example, some wires will be slightly longer than others. In practice; however, the probes are paired such that they generally match to within 0.05 ohm. Thus each wire will assume slightly different values for m , and thus slightly different values for Θ_{ave} . Of course the thermosonde automatic balance circuitry will subtract out any constant (or low frequency) difference in the average temperatures (resistances) between the probes. Thus the slowly varying elevated probe temperature and the small differences between the two probes will not cause enhanced signals.

A possible mechanism that could introduce artifact resides is the expression for "m". Since "m" is a function of the heat transfer coefficient, an AC or high frequency effect could result from fluctuations in velocity (Reynold's number). That is:

$$h_2 = h_1 \times \left(\frac{v_2}{v_1} \right)^{.33} \times \left(\frac{r_2}{r_1} \right)^{-.67} \quad (22)$$

A fixed difference between h_1 and h_2 results from the differences in wire size but a perturbation results from small fast changes in the wind speed occurring at each probe, that is, velocity turbulence. In other words, if each probe is heated above the ambient by solar radiation, then fluctuations in wind speed can induce small fluctuations in "h" and consequently "m" and ΔT . To assess the magnitude of this effect, computer simulations of Eq. (21) were devised that allowed for realistic geometrical differences between the probes. Separate computer runs increased the support temperatures (Θ_0 varied from 0. to 10. °C). To simulate the effects of temperature turbulence on the probes, sets of uniform random numbers between the values of -1 and +1 were generated (100 random numbers per set). Each set was then multiplied by a constant (about 0.002). RMS differences between two air temperatures generated in this way provided a simulation of C_T (RMS). In practice, we multiplied the sets of numbers by appropriate integers (1 to 10) to obtain a C_T (RMS) from 0.002 to 0.02°, which is the range normally encountered in any profile measurement. A similar procedure was employed to generate random values of velocity fluctuations of about 2 percent. Our measurements lead us to believe that fluctuations in velocity of 2 percent constitute strong mechanical turbulence.

Computer logic was developed that provided a means to examine extreme conditions. For example, we wished to compare the effects of: 1) correlated against uncorrelated air temperature

fluctuations at the two probes, and 2) allowing the velocity fluctuations to correlate (or anti-correlate) with the temperature fluctuations. Thus sets of correlated, anti-correlated, and, uncorrelated random ΔT 's and Δv 's were generated that provided simulated values of C_T , "h", and "m", and ultimately DC and AC differences between the simulated wire pairs. For example, one run computed different sets of random numbers for the temperature and velocity fluctuations. Also the sign (positive or negative) of each of the fluctuations was determined from independent sets of random numbers. Separate sets were calculated for each probe. Thus, for this particular case, there was no correlation in the fluctuations of any of the different simulations. A second example used different sets of random numbers to calculate the temperature fluctuations and the sign of the fluctuations at each probe but required that: a) the level of temperature and velocity fluctuation to be the same, and b) require an equal but opposite fluctuation at the other probe. The average differences between the two wires were obtained by invoking Eq. (21). Table 22 shows the results of these two simulations. Clearly, the average wire temperature exceeds the ambient by about 0.5°C and the DC temperature difference between the wires is of the same order of magnitude as the thermal noise (approximately 0.002°C). These DC differences, however, are nulled by the electronics and do not contribute to the measurement of the fluctuations. Air temperature fluctuations, and to a small extent, solar heating, together with velocity fluctuations, do contribute to the temperature fluctuations in the wire. Figures 11 and 12 illustrate the

Table 22. Estimation of Differences between RMS Air Temperature Fluctuations and RMS Wire Temperature Fluctuations by Simulation of Temperature and Velocity Fluctuations by Random Numbers and Consideration of Wire Temperature Distribution.

Case 1 (No Correlations)			Case 2 (With Correlations)		
$C_{T,air}$ (RMS) $\times 10^4$	$C_{T,wire}$ (RMS) $\times 10^4$	DIFF. $\times 10^4$	$C_{T,air}$ (RMS) $\times 10^4$	$C_{T,wire}$ (RMS) $\times 10^4$	DIFF. $\times 10^4$
17	20	-4	20	3	17
36	35	1	38	14	24
57	52	5	62	33	29
74	67	7	79	49	30
91	80	11	93	62	31
104	90	14	122	86	36
122	105	17	132	96	36
144	125	20	157	117	40
139	122	16	176	134	42
181	155	26	199	153	46

Average air temperature = -60.°C.
 Support temperatures = -56.°C.
 DC difference between average air and wire temperatures = 0.654°C.
 DC temperature difference between the wires = .0027°C.

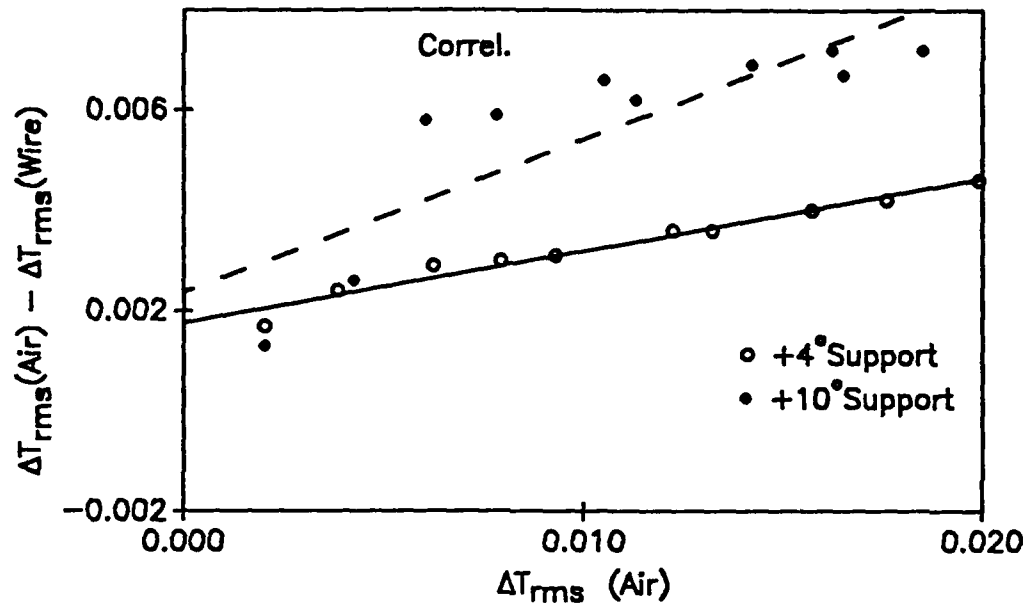


Figure 11. Random Number Computer Simulation of Difference between Air and Wire RMS Temperature Variations between Probes as a Function of RMS Air Temperature Variation with Random Numbers Uncorrelated in Terms of Fluctuations in Temperature and Velocity at the Probes.

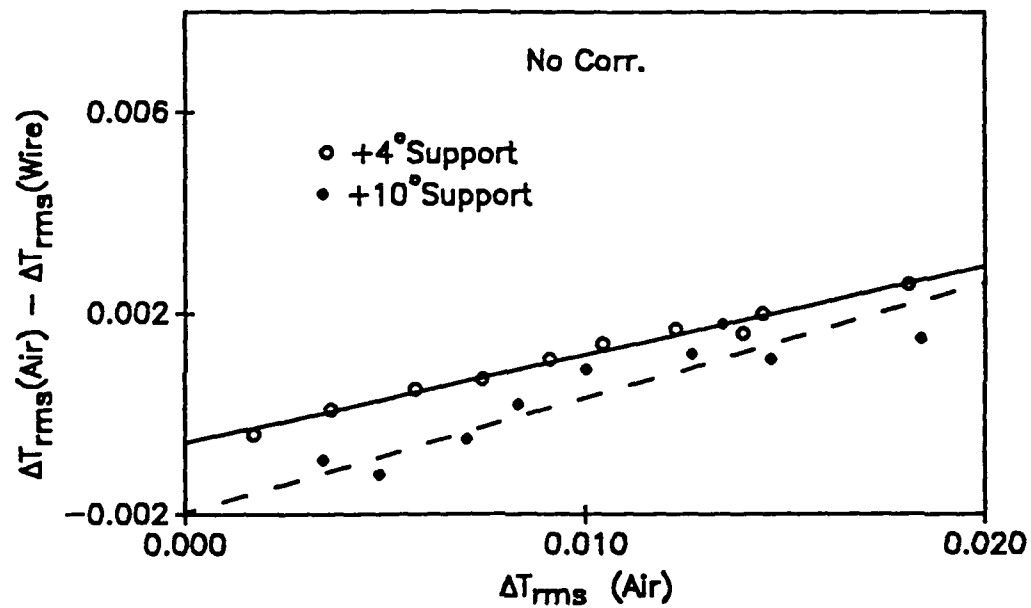


Figure 12. Random Number Computer Simulation of Difference between Air and Wire RMS Temperature Variations between Probes as a Function of RMS Air Temperature Variation with Random Numbers Correlated in Terms of Fluctuations in Temperature and Velocity at the Probes.

difference between the RMS difference of air temperature between the probes and the RMS difference of wire temperature. Under typical conditions, this difference increases as the RMS air temperature increases; the correlated case shows larger differences than the uncorrelated case and the correlated case shows greater effect due to changes in support temperature.

We have used examples of 4°C and 10°C elevated support temperatures. Although our calculations and measurements have indicated that the probe body can be heated to this extent in the daytime, reduced conduction and lower temperatures certainly will occur at the needle tips where the fine wires are attached to the probes. Also, we do not think that the instantaneous fluctuations of the ambient air data is very highly correlated between the probes. It thus appears that any induced RMS probe effect from mismatched wires, solar heating, or mechanical turbulence will not exceed the noise limit of about 0.002°C. The simulations indicate that it is unlikely that the observed diurnal effect is due to artifact produced by solar heating or mechanical turbulence. Of course if conditions were more extreme, (greater geometrical mismatch, higher support temperatures, larger velocity fluctuations, smaller heat transfer coefficient, etc.) then larger probe effects would be noticeable.

5.2 Special In-Situ Balloon Experiments

As mentioned earlier, several balloon experiments were devised to test the hypothesis that solar heating caused elevated ΔT , BLS, and C_T^2 . Two of these experiments will be discussed here. The first experiment consisted of a series of thermosonde payloads that carried specially painted and/or taped probes. Some pairs of probes were taped with high emittance metallized mylar. Other probes were painted white, while other pairs were painted black or left unpainted. Another set had one white probe and one black probe. If the hypothesis that solar heating causes the diurnal effect is correct, then the black (hotter) probes should show evidence of larger ΔT , BLS, and C_T^2 . The second experiment consisted of "long wire" thermosonde probes. If "end effect" (hot needles) caused elevated average wire temperatures with its subsequent sensitivity to velocity turbulence, then longer wires would reduce the average temperature rise in the wire and lower its sensitivity to velocity fluctuations.

As a control, each test flight was compared to a flight that had plain, unpainted, stainless steel (SST) probes. The measured profile for this "control" flight is shown in Figure 13. Note that the dots on this and the following profiles are the 4-second RMS measurements of C_n^2 . Since the balloon ascends at about 5 m/s, on average, each point represents a 20-meter RMS measurement. The solid smooth curve, which results from the C_T noise limit of 0.002°C, shows the thermosonde C_n^2 noise limit as a function of altitude. An overlay of a Gaussian smoothed profile having a 40 meter standard deviation is shown by the variable solid curve. Both the 20 meter data and the smoothed profile clearly show the daytime stratospheric C_n^2 enhancement.

We now describe the special configurations of the various test flights. Two flights, whose profiles are shown in Figures 14 and 15, were configured with probes whose shafts were taped with highly reflective metallized mylar²⁷. On average, the tape was tested to have an absorptance of 0.14 and an emittance of 0.80. The effects of radiation should be reduced substantially for the high ratio of emittance to absorptance. Since the needles (standoffs) in Figures 14 and 15 were

²⁷Sheldahl Corp. part number 7SG400800-010, specification number G400800.

L0948
LAUNCH: 02-13-87 20:00:50 UT

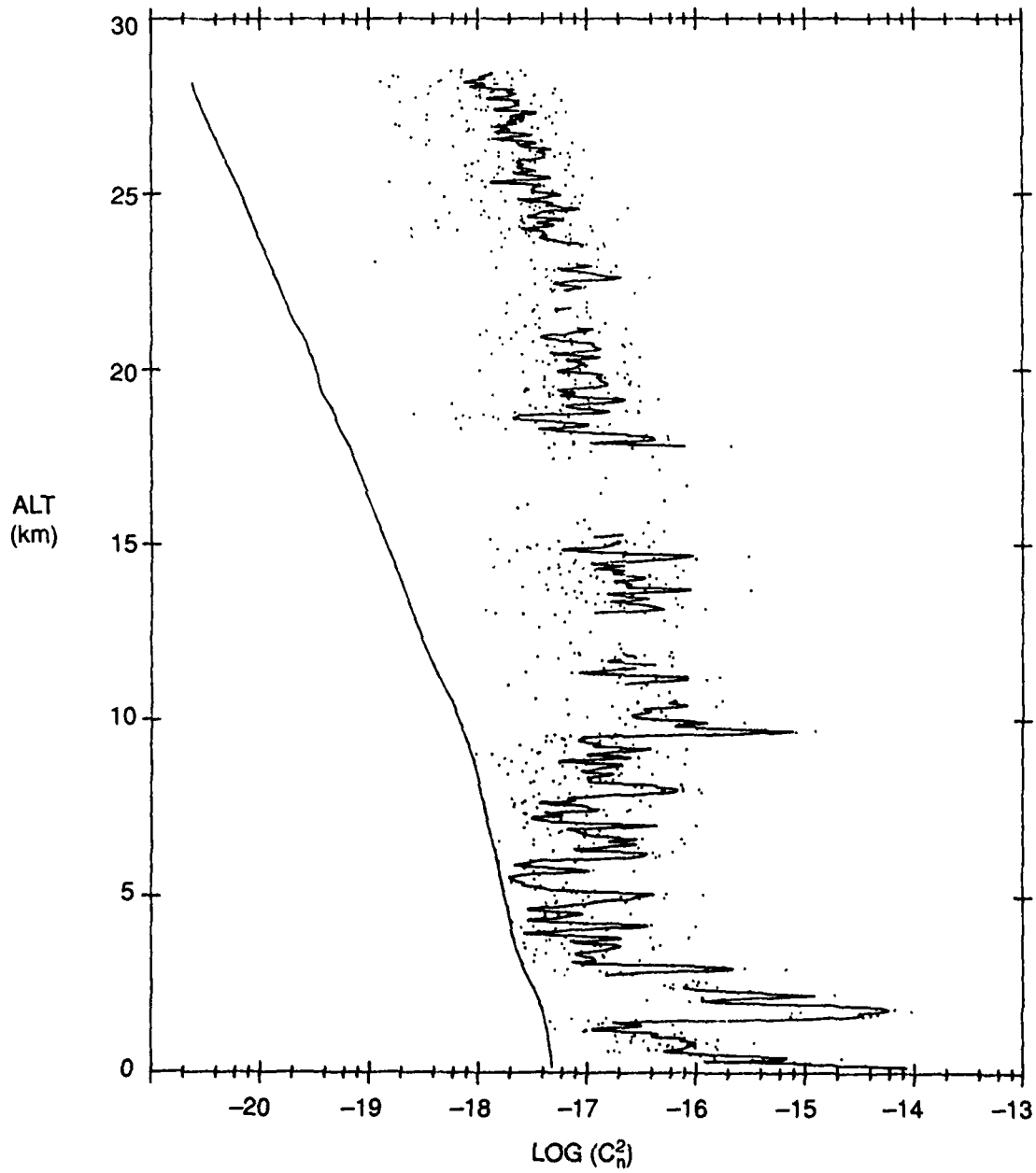


Figure 13. Thermosonde C_n^2 Profile (L0948) as a Function of Altitude for Plain, Unpainted Stainless Steel Probes.

L0949
LAUNCH: 02-18-87 20:49:45 UT

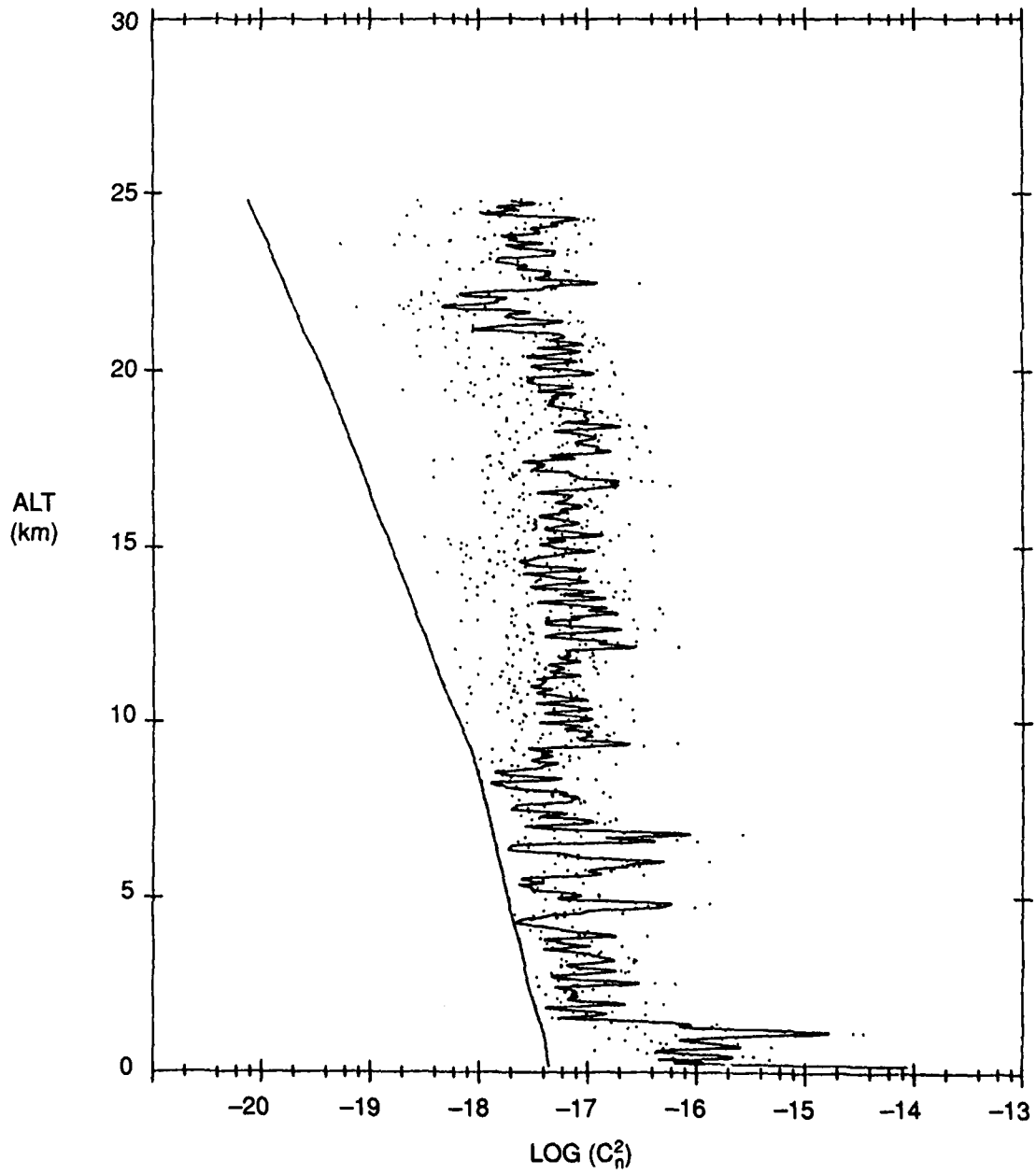


Figure 14. Thermosonde C_n^2 Profile (L0949) as a Function of Altitude for Taped but Unpainted Stainless Steel Probes.

L0957
LAUNCH: 02-27-87 20:37:37 UT

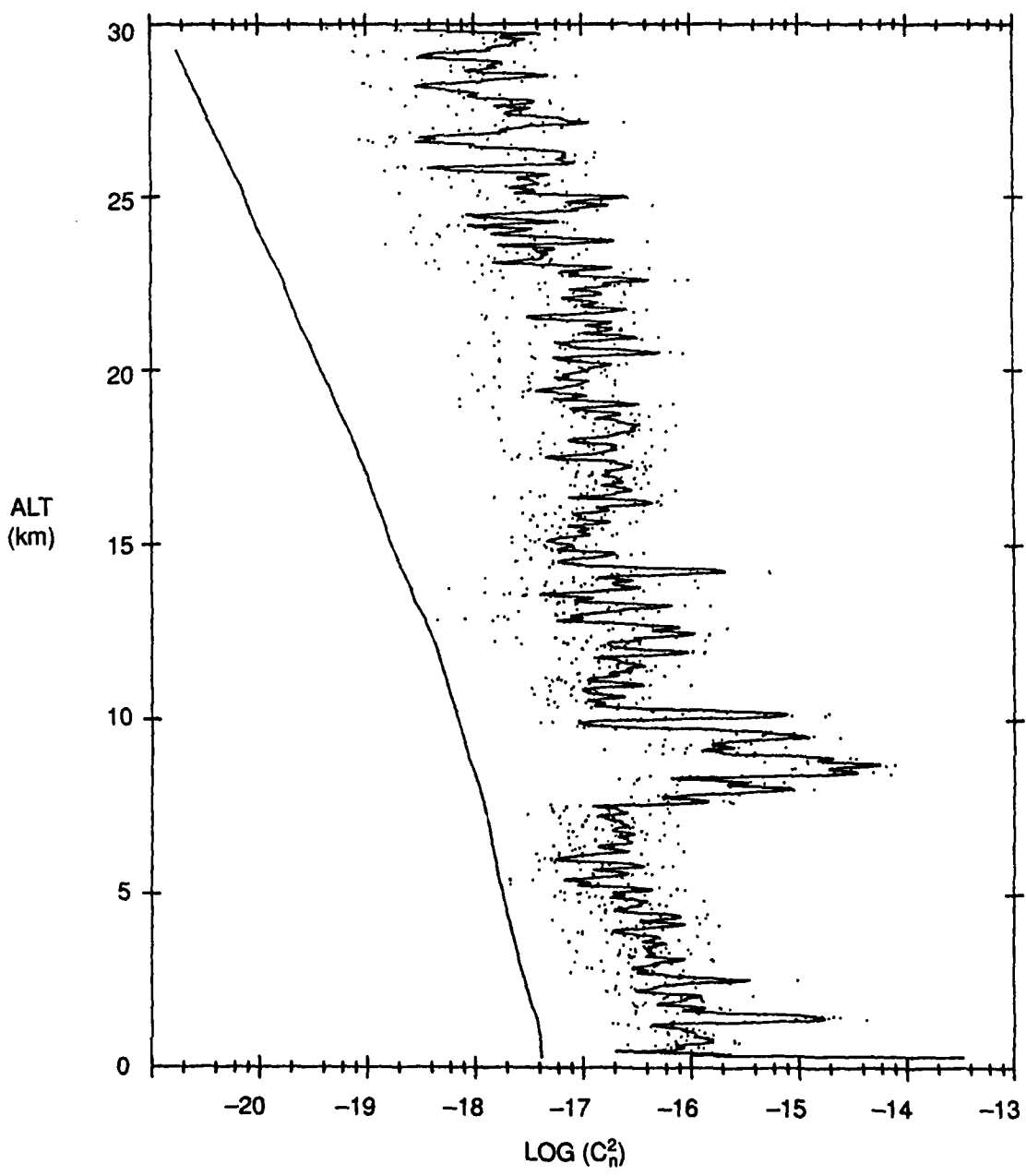


Figure 15. Thermosonde C_n^2 Profile (L0957) as a Function of Altitude for Taped but Unpainted Stainless Steel Probes.

L0961
LAUNCH: 03-03-87 20:04:03 UT

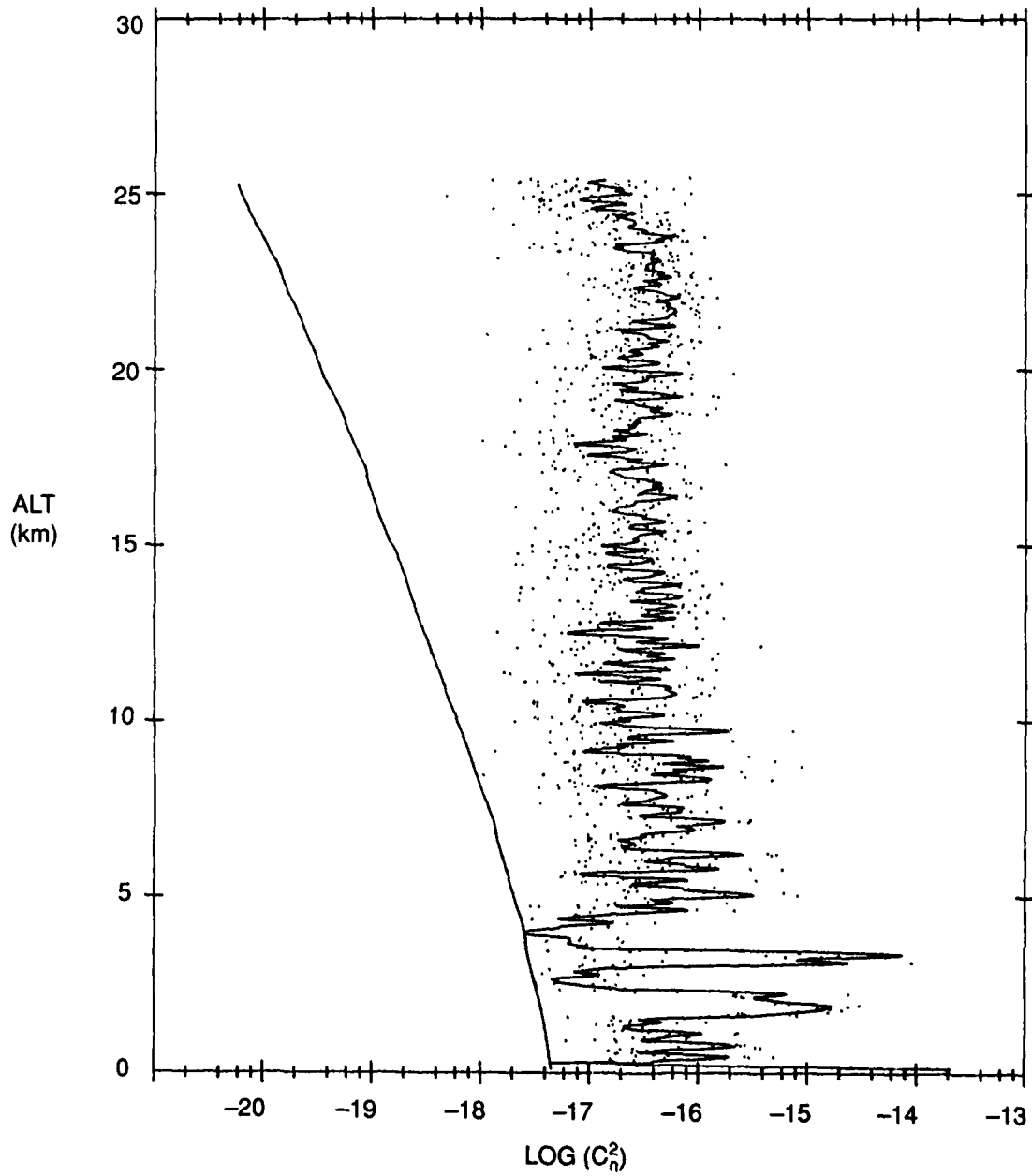


Figure 16. Thermosonde C_n^2 Profile (L0961) as a Function of Altitude for Taped and White Painted Stainless Steel Probes.

L4023
LAUNCH: 03-11-87 21:26:17 UT

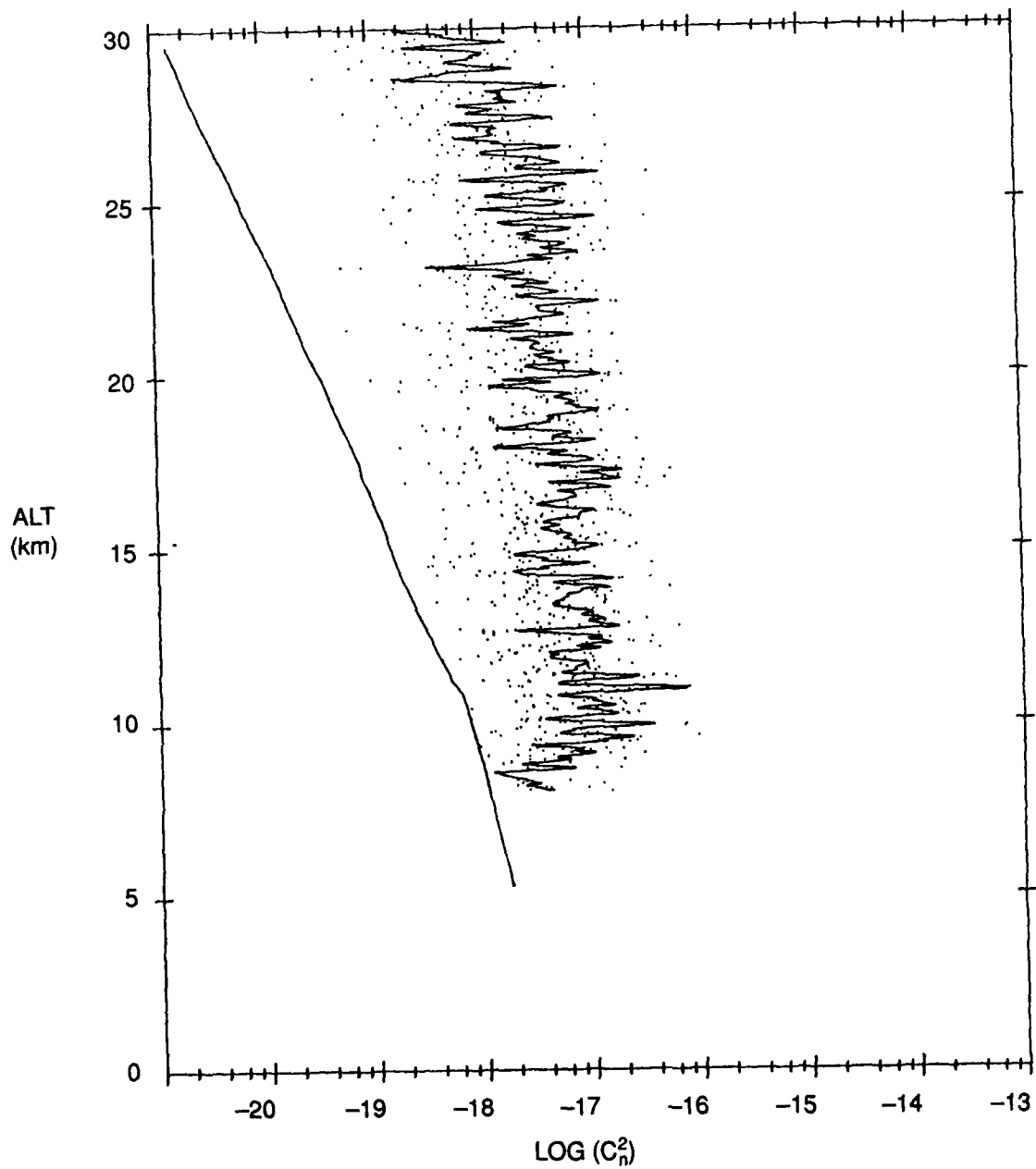


Figure 17. Thermosonde C_n^2 Profile (L4023) as a Function of Altitude for Black Painted Stainless Steel Probes.

L4021
LAUNCH: 04-14-87 16:15:01 UT

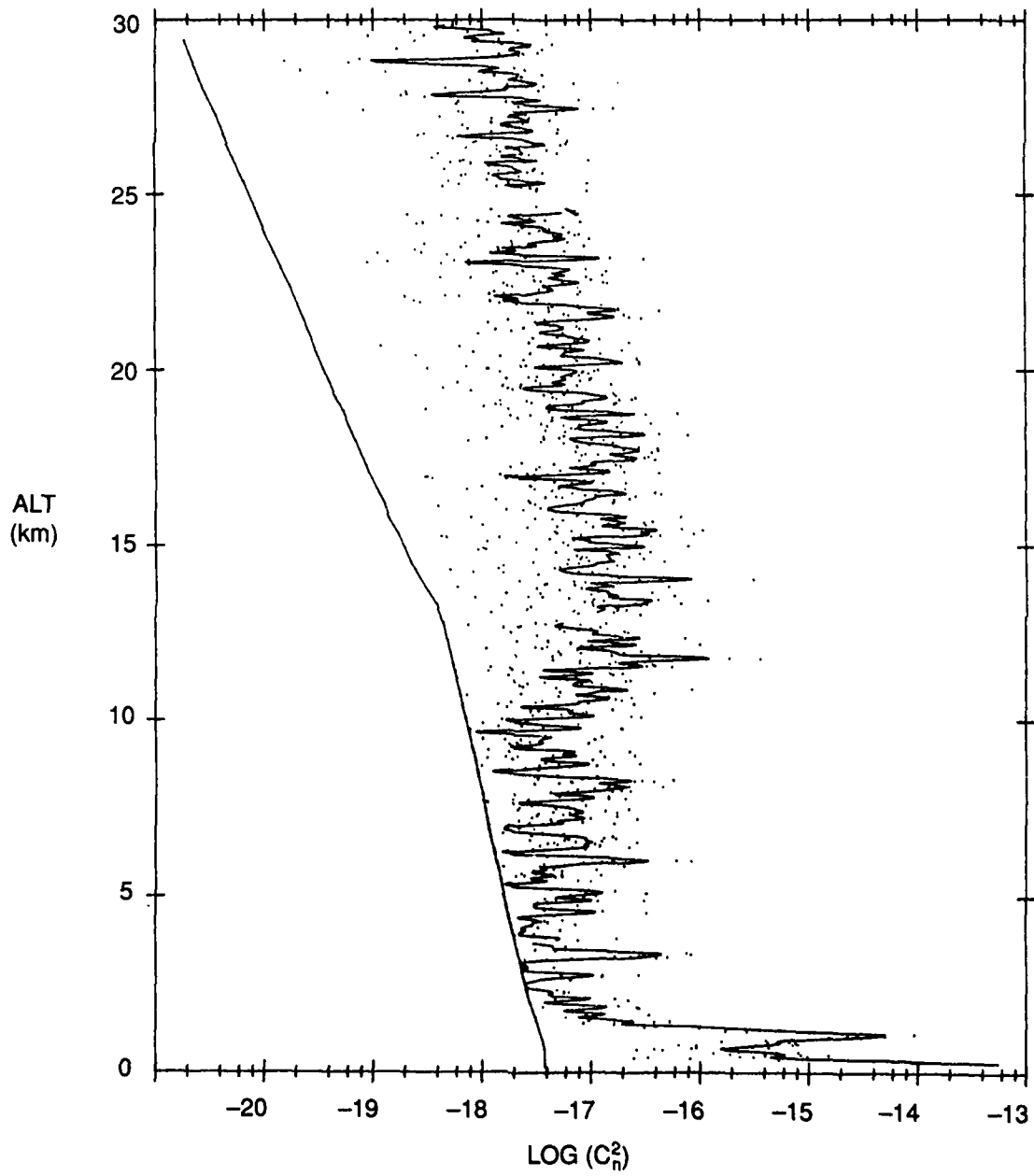


Figure 18. Thermosonde C_n^2 Profile (L4021) as a Function of Altitude for Taped and White Painted Stainless Steel Probes.

L4024
LAUNCH: 04-14-87 19:56:32 UT

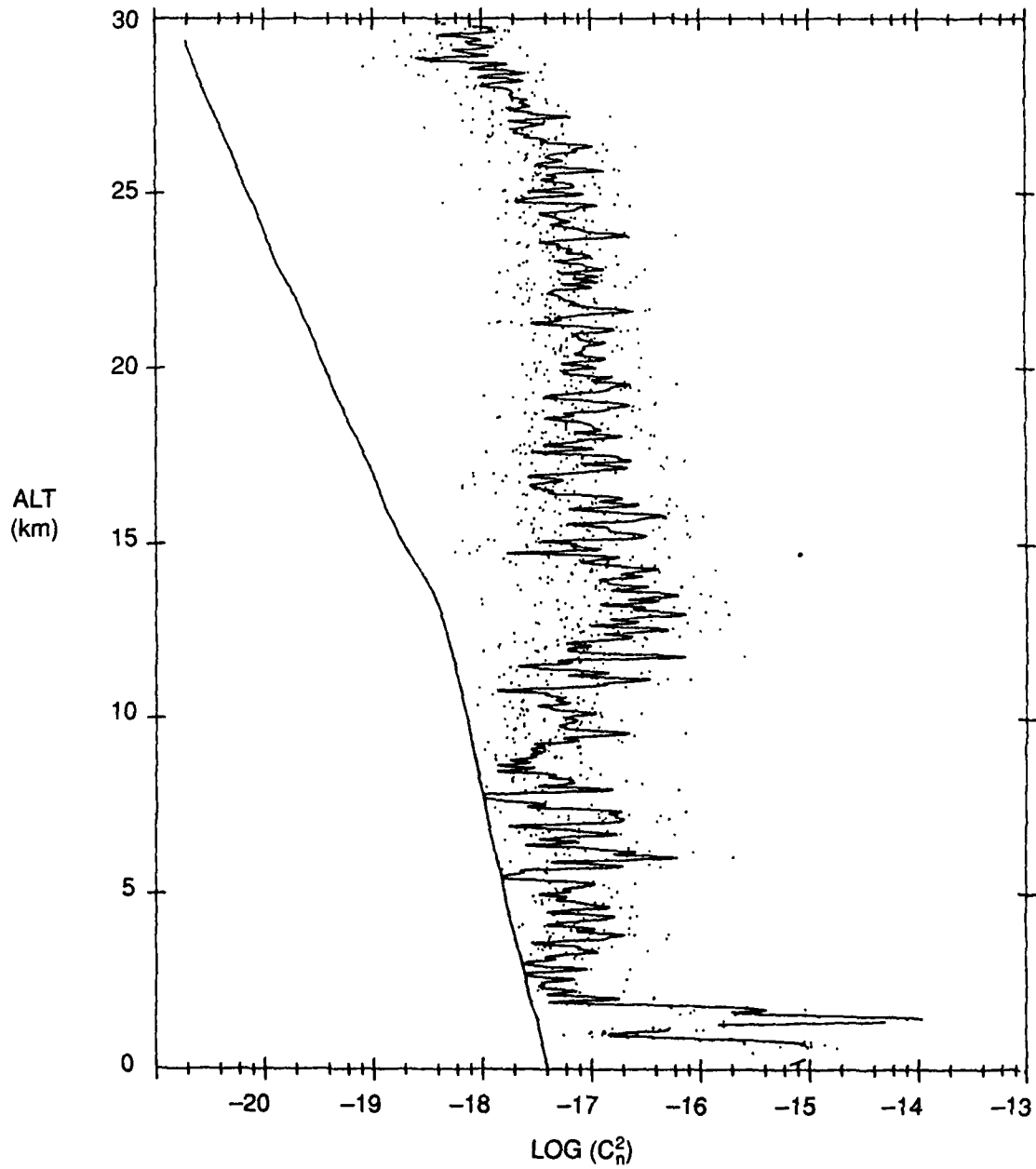


Figure 19. Thermosonde C_n^2 Profile (L4024) as a Function of Altitude for Black Painted Stainless Steel Probes.

not taped, two additional taped probe flights were launched (Figures 16 and 18) whose needles were painted with white glossy enamel. To attempt introducing a large artificial heating effect, two more flights, as depicted in Figures 17 and 19, were launched with pairs of probes that, except for the fine sensor wire, were completely painted flat black. An even larger differential effect could be expected if one probe were taped and had white needles and the paired probe were painted black. Such a configuration was launched and it is shown in Figure 20. Three additional test flights were launched. One (Figure 21) was a test to reduce end effects by increasing the fine wire length by three times its normal length. Another flight (Figure 22) having a 400 foot launch train (separation between balloon and thermosonde) was launched to determine if the daytime enhancement were due to the sensor being in a thermal shedding wake from the balloon. If the enhancement were caused by balloon heating and thermal shedding, then a much longer train will place the thermosonde further from the source and thus reduce any wake effect. The last flight was launched to test the thermosonde electronic circuit for changes in gain or sensitivity due to the cold stratospheric temperatures. This test flight (Figure 23) consisted of replacing the fine wire probes with precision, low temperature coefficient, fixed resistors. Figure 23 clearly shows that no baseline shift occurs from the electronics itself.

In order to visually compare these test flights, 500 meter arithmetic running averages were calculated. Each profile is plotted and compared to the "control" (plain SST, S/N L0948) profile in Figure 24. Although the visual comparisons are somewhat subjective, we interpret them to indicate that no apparent influence in the enhancement can be attributed to changing the emittance to absorptance ratio. The black probes (S/N L4023 and L4024) show no greater effect than the taped (S/N L0949 and L0957) or taped/white probes (S/N L0961 and L4021). The black and white pair (S/N L4020), which should be the worst case, also shows no greater enhancement. Significantly, the long wire probes (S/N L1016) did not appear to have any influence in reducing the daytime enhancement. Finally, the very long train payload (S/N L0952) also did not appear to lessen the daytime enhancement. A more quantitative comparison may be made by inspecting the differences in the calculated isoplanatic angles for these flights. Table 23 lists the values of the isoplanatic angle, θ_0 , with a brief description of the configuration. We note that the configuration having taped probes but unpainted needles fell at both extremes, having both the smallest and largest values of θ_0 . The black probes, which if radiation is a problem, should have small θ_0 . Contrary to this expectation however, they have (one in particular) large θ_0 (weak C_n^2). The long wire probe, lying in the center of the range, is inconclusive while the long train flight has a fairly small value for θ_0 for a maximum altitude of only 12 km. We conclude therefore that these test flights do not seem to support the hypothesis that solar radiation with ensuing probe heating causes the observed diurnal variation in the stratospheric C_n^2 profile.

L4020
LAUNCH: 04-15-87 20:10:29 UT

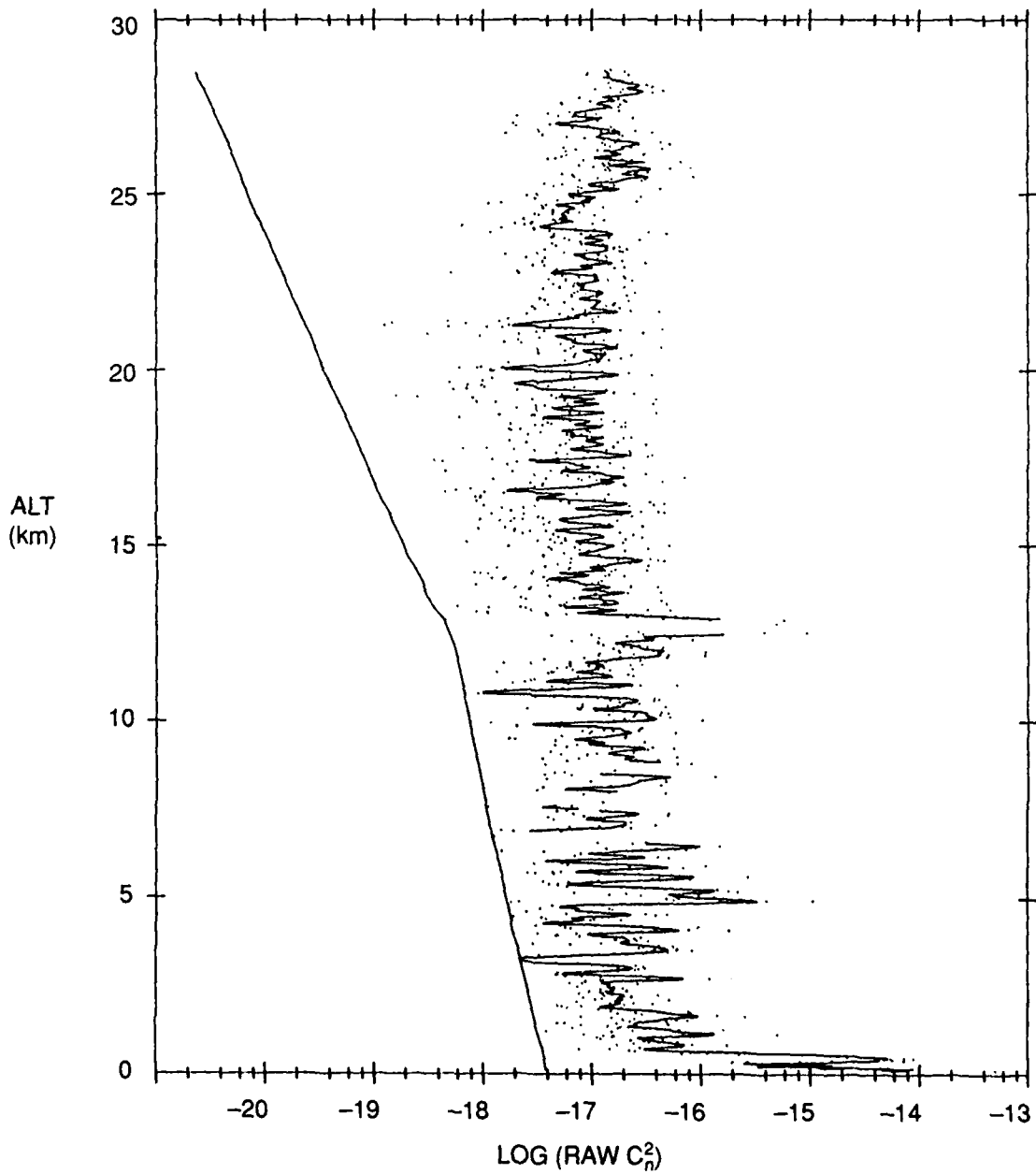


Figure 20. Thermosonde C_n^2 Profile (L4020) as a Function of Altitude for One Black Painted Stainless Steel Probes and One Taped and White Painted Stainless Steel Probe.

L01016
LAUNCH: 07-15-87 15:03:24 UT

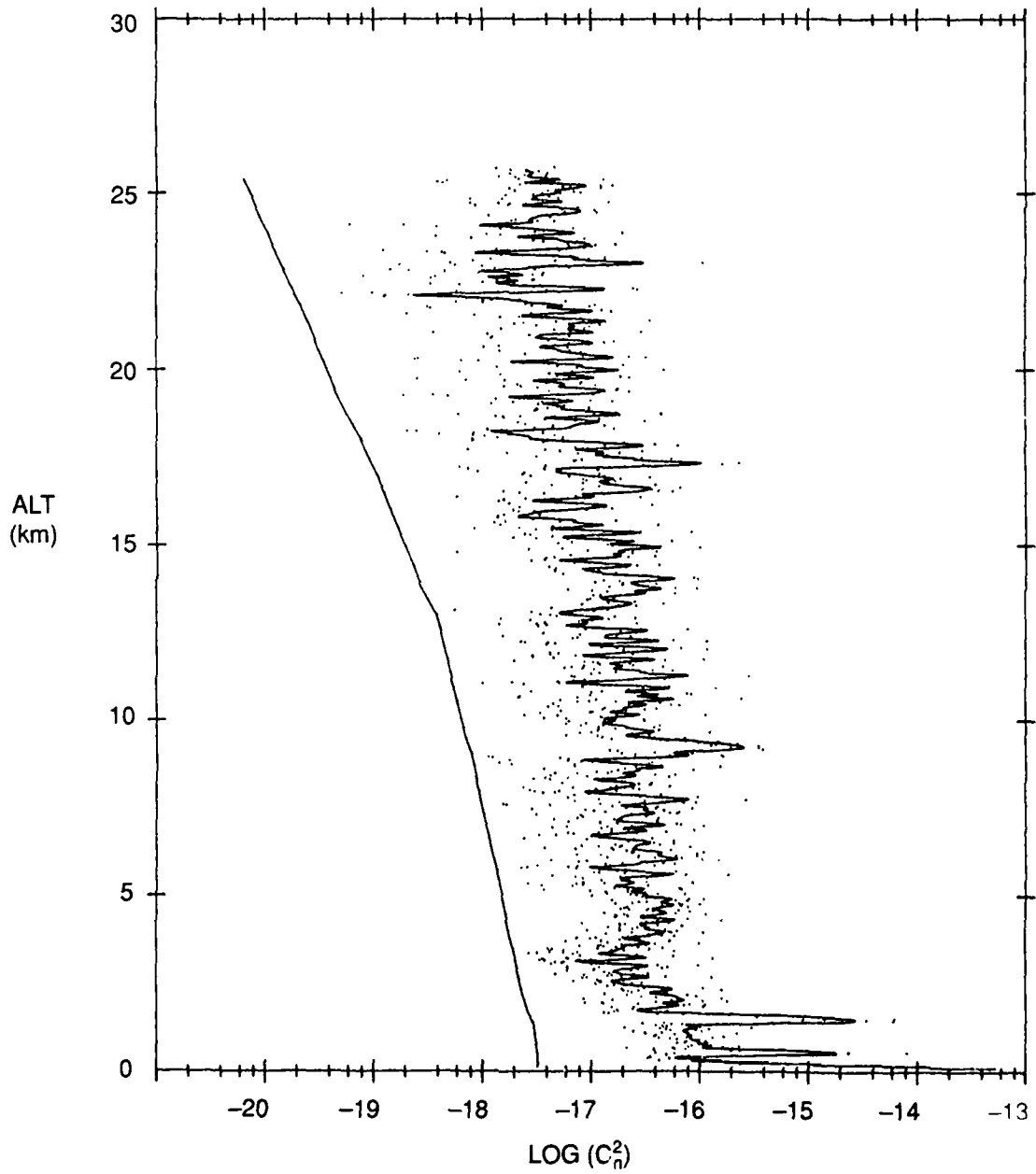


Figure 21. Thermosonde C_n^2 Profile (L1016) as a Function of Altitude for Long Wire Unpainted Stainless Steel Probes.

L00952
LAUNCH: 07-17-87 06:11:17 UT

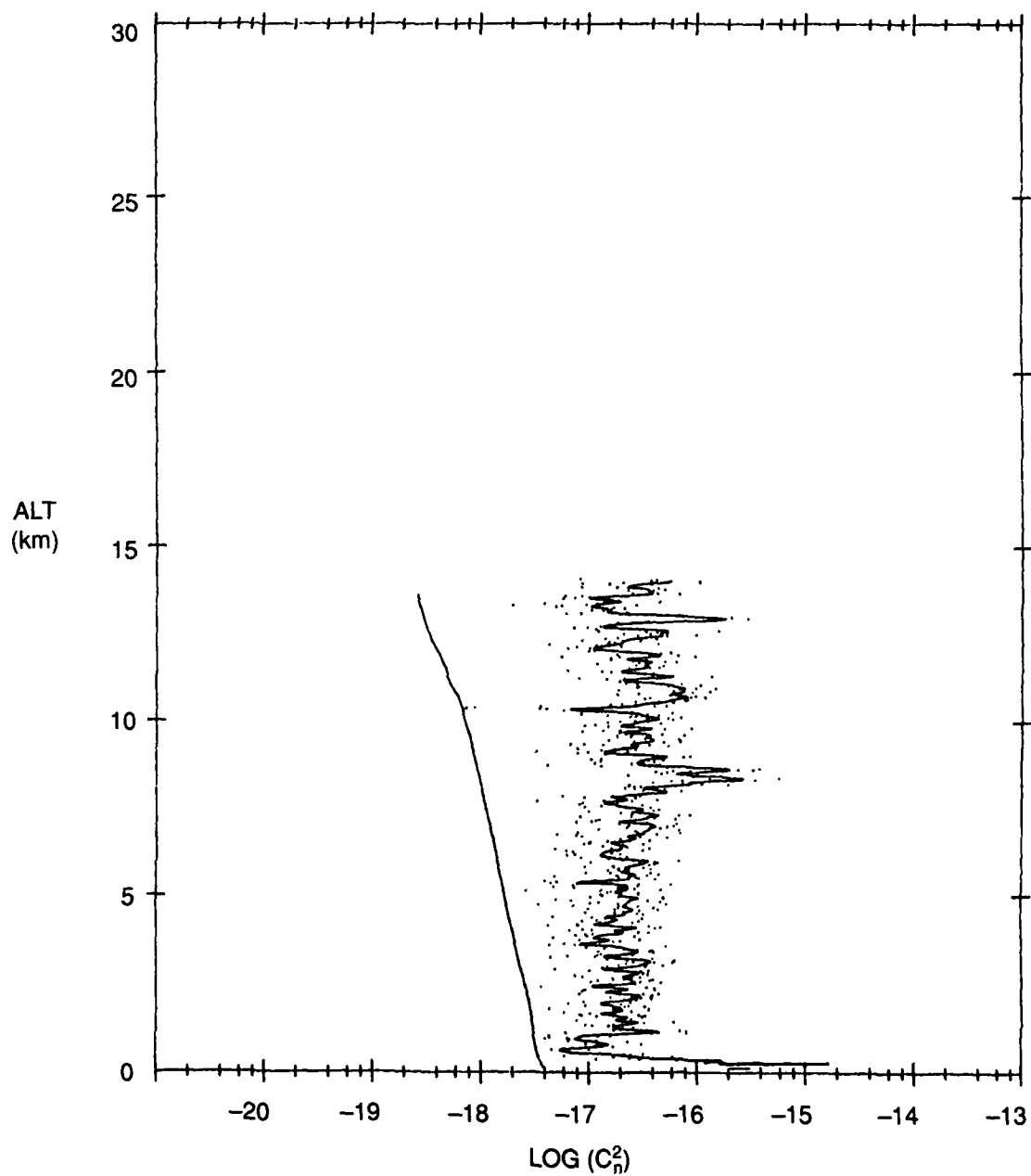


Figure 22. Thermosonde C_1^2 Profile (L0952) as a Function of Altitude for a Very Long Balloon Train and Thermosonde Having Plain Unpainted Stainless Steel Probes.

L1019
LAUNCH: 05-08-87 15:38:02 UT

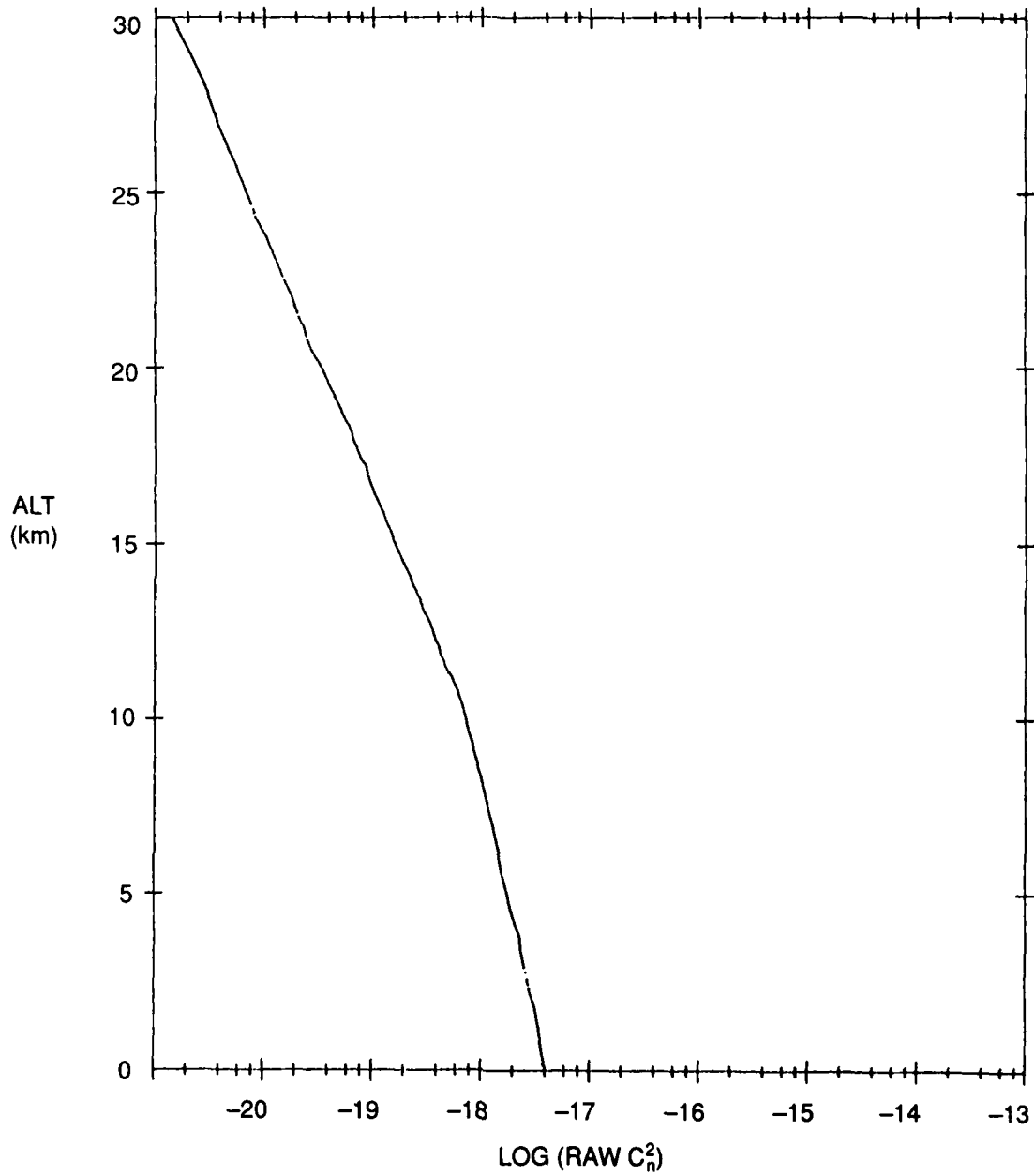


Figure 23. Thermosonde C_n^2 Profile (L1019) as a Function of Altitude for Fixed Low Temperature Coefficient Resistors Substituted in Place of the Normal Probes.

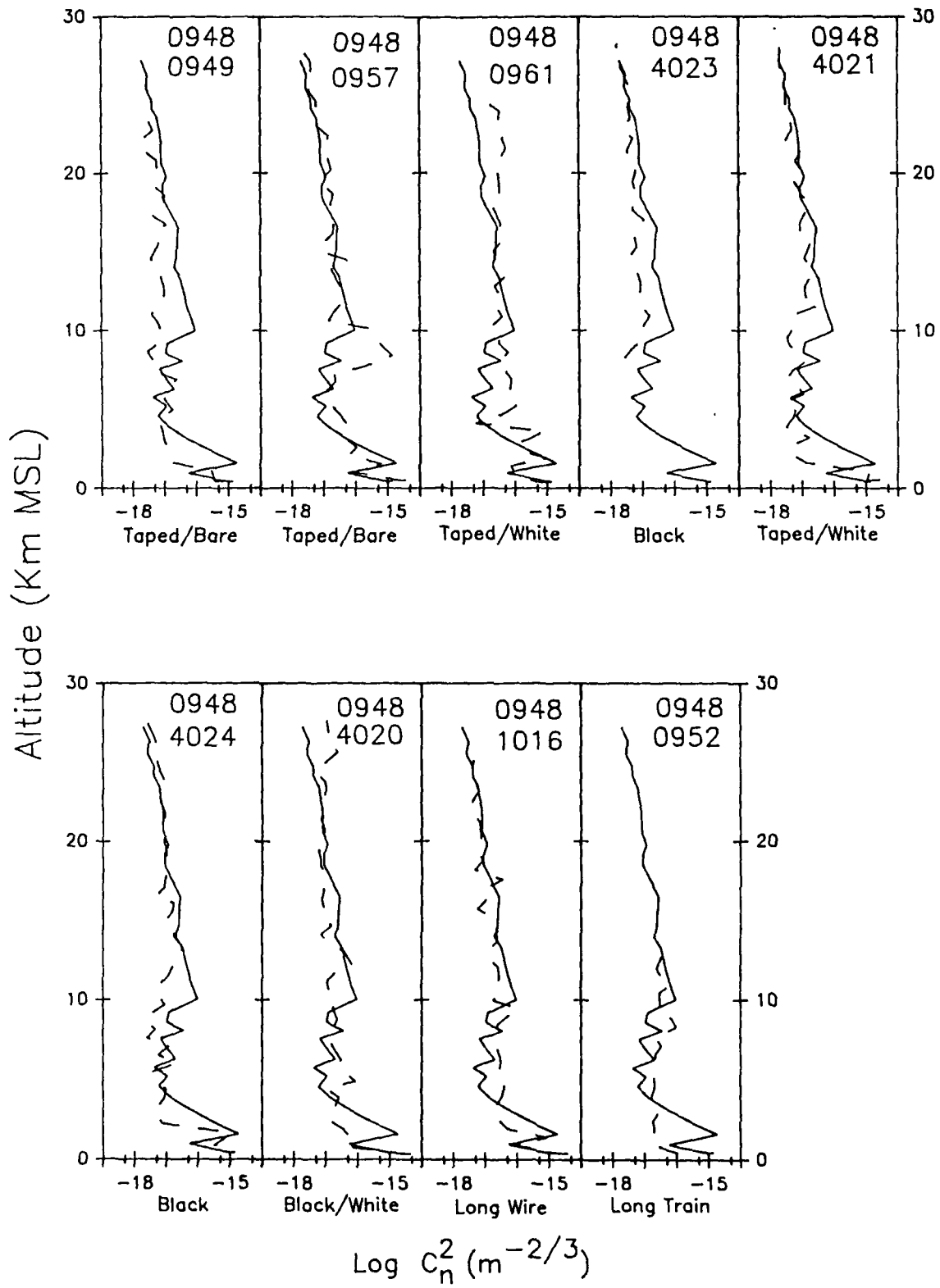


Figure 24. Comparison between the variously configured thermosonde flights.

Table 23. Specially Configured Thermosondes— Effect on the
Isoplanatic Angle, θ_0 . θ_0 measured in (μ rad) at 0.3 μ m.

θ_0	S/N	Comment:
0.8	L0957	Taped Probes/No Paint
1.1	L0961	Taped Probes/White Painted Needles
1.4	L4020	1 Taped/White Probe, 1 Black Probe
1.6	L0948	Plain Stainless Steel Probe
2.0	L1016	Long Wire Probes
2.0	L4024	Black Painted Probes
2.3	L4021	Taped Probes/White Painted Needles
2.6	L0952	Long Train (12 km Max. Altitude)
3.0	L4023	Black Painted Probes
3.3	L0949	Taped Probes/No Paint

5.3 Low Density Chamber Experiments

A series of laboratory experiments were devised to investigate the responsivity of the thermosonde sensors to radiation at stratospheric pressures. A randomly selected thermosonde package was placed inside a large vacuum chamber (3 m \times 3 m right cylinder) with a probe separation of 0.5 meter. No modifications were made to the thermosonde probes for these experiments. Ten-inch diameter windows were used to introduce radiation from a high power (1000 Watt), FEL type quartz-halogen tungsten filament lamp. This lamp was used in both a long pulse and continuous fashion to simulate both low and high frequency changes. An adjustment to the reflector allowed the lamp to flood the probes fairly evenly. Entrance and exit windows allowed a clear view into the chamber and allowed detection of strong heat radiation exiting the chamber.

In the first experiment, the chamber was operated at 1 atmosphere pressure. The chamber doors were tightly closed, and, after the air in the chamber achieved equilibrium with the wall temperature, and all detectable motion settled out, the lamp was pulsed on and off for periods of 45 seconds. Figure 25 (Upper Plot) shows the thermosonde measured value of C_n^2 as a function of time. With the lamp turned off, the thermosonde measured its noise limited value of about 2×10^{-17} ($m^{-2/3}$). Turning the lamp on or off introduced a transient response as seen by the bumps in the time series. The lower plot in Figure 25 shows a similar effect, but in this case the chamber pressure was reduced to 30 mbar. At the lower pressure the thermosonde noise limit is lowered to about 1×10^{-20} ($m^{-2/3}$) thus the transient response is emphasized on the logarithmic plot. We are not particularly concerned about the transients because: 1) we expect steady solar illumination on the probes in flight and, 2) the longer term effect settles out due to the automatic balancing feature of the electronics bridge circuitry.

In the next series of experiments, a slow air leak was introduced into the chamber. Although the pressure increased very slowly, the leak provided a level of turbulence at the probes. Figure 26 (upper and center graphs) shows the result of pulsing the lamp on for 15 seconds and then

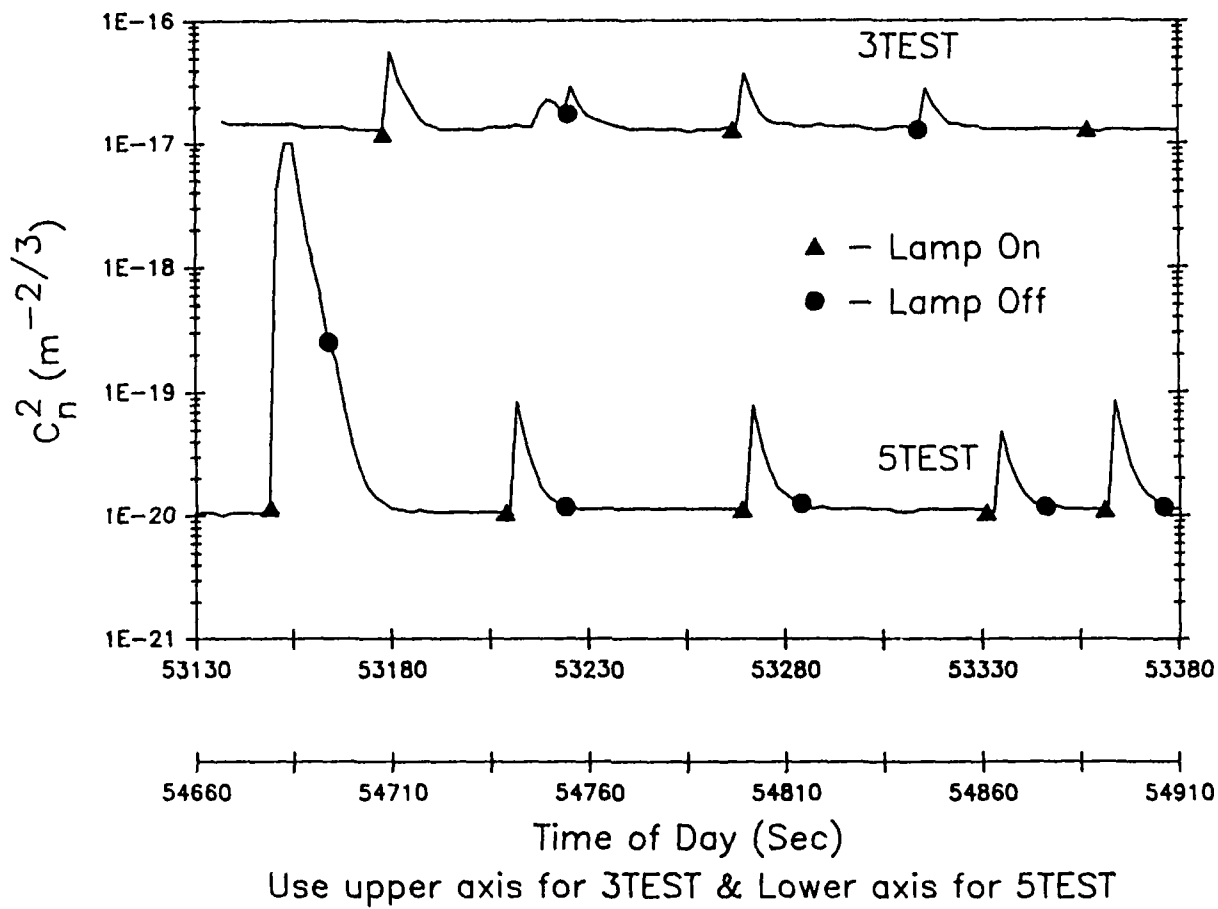


Figure 25. Transient Response of Thermosonde to "Switched" Radiation in a Laboratory Chamber.

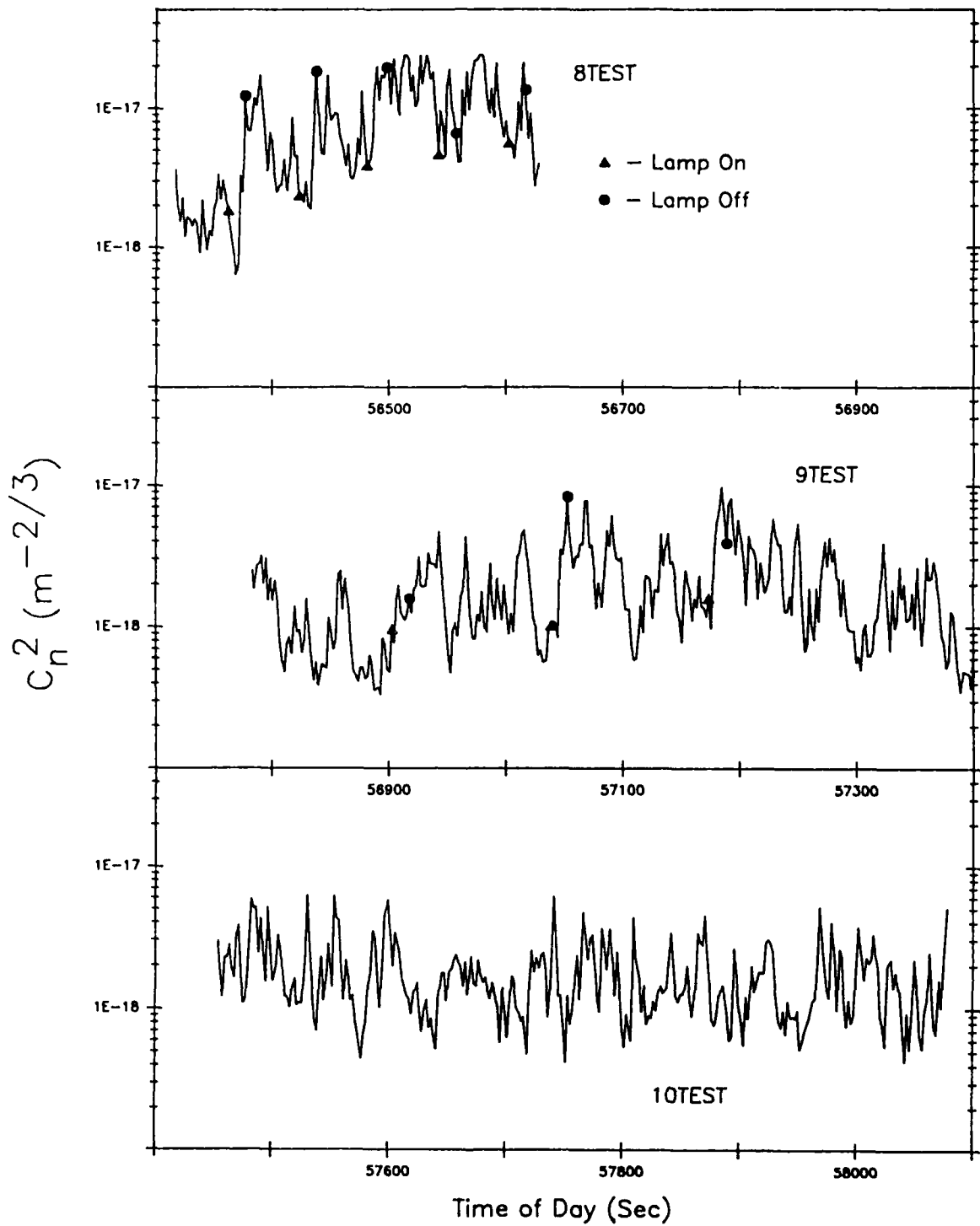


Figure 26. Response of Thermosonde to "Switched" Radiation in a Laboratory Chamber at Stratospheric Pressures.

switching it off for several minutes. Since the switching times seem to correlate with peaks in the time series, it appears that transients may be introduced at those times but no definite increase in the level of turbulence can be attributed to the radiation. The lower graph in Figure 26 shows the turbulence time series alone with no radiation. Evidently the measured level of turbulence remains the same regardless of the illuminating radiation.

The thermosonde electronics itself has been subjected to numerous and repeated thermal low pressure chamber experiments^{28,29,30} to test for electronic temperature sensitivity. The graphs in Figure 27 indicate the ranges of air temperature and electronic circuit board temperature that the devices encounter throughout their ascent from the ground to the balloon burst altitude of about 30 km. The upper graph shows the electronics board temperature at a point near the power regulator (the hottest spot on the board). In the stratosphere, where the BLS dominates, the temperature is quite acceptable, ranging from 10° to 22°C. The lower graph shows the electronics board temperature at a point near one of its corners, far from the regulator (the coldest spot on the board). Again in the stratosphere, the temperature at this point ranges from -10° to -25°C.

The graphs in Figure 28 show the thermosonde low and high gain calibration curves at various chamber temperatures (upper and lower plots respectively). Calibration values of $\Delta T \times R_0$ are plotted against the measured output voltages. As the plots indicate, the calibration is quite linear down to very small values and it is quite insensitive to temperature down to -30°C. As a consequence of these tests, a few electronics components (a couple of resistors, capacitors, and IC's) were discovered to contribute to the small temperature sensitivity. Those components were replaced in all future flights by very low temperature coefficient components but the diurnal effect remained unchanged. We do not, therefore, consider electronic sensitivity to temperature as a likely source of the BLS.

²⁸Murphy, G.P. (1981) *New Techniques and Devices for Measuring Stratospheric Winds and Turbulence*, AFGL-TR-81-0128, ADA102680

²⁹Brown, J.H., et. al. (1982) *Sonde Experiments for Comparative Measurements of Optical Turbulence*, AFGL-TR-82-0079, ADA118740

³⁰Hills, R.S. (1982) *Research, Design and Development Study to Measure Atmospheric Optical Turbulence*, AFGL-TR-82-0334, ADA123392

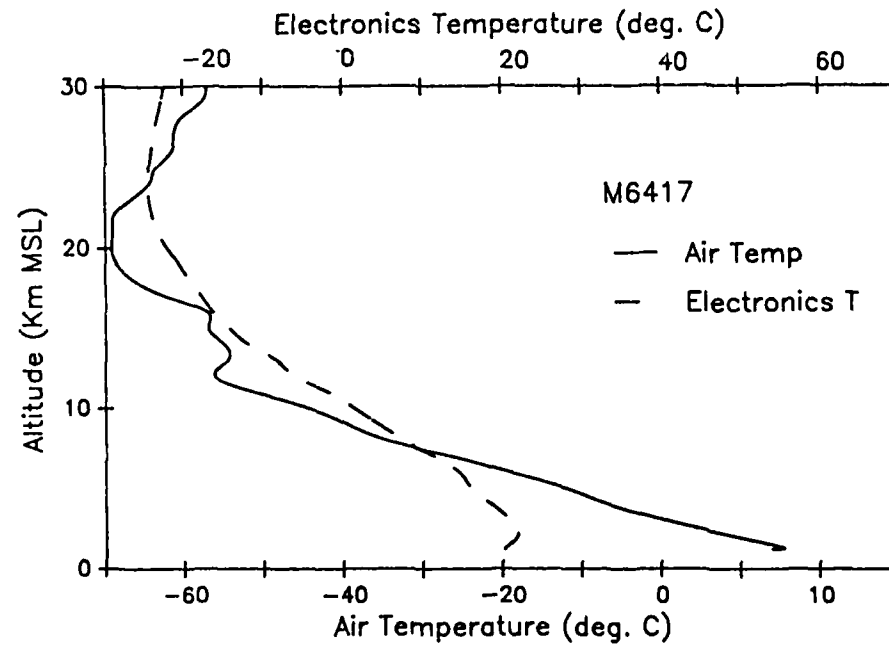
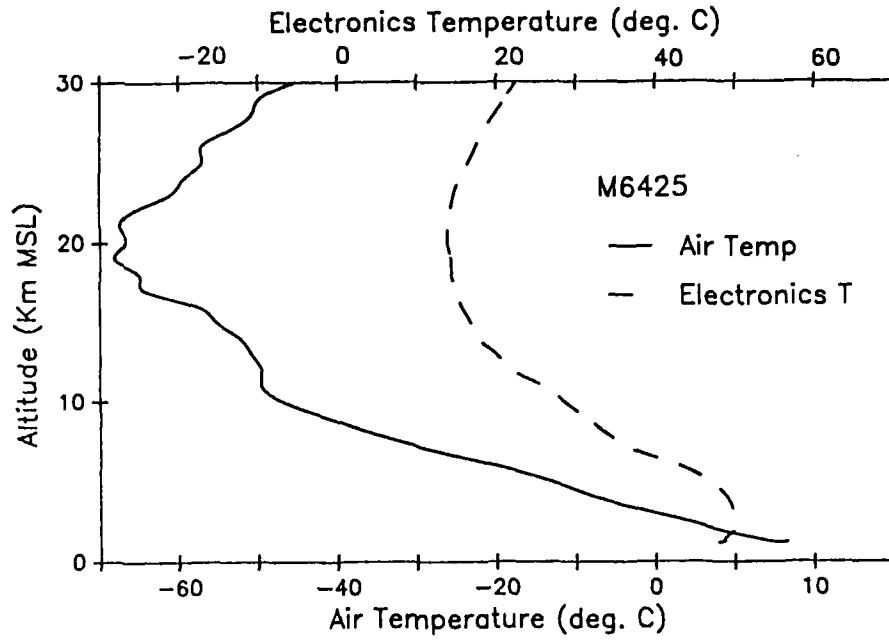


Figure 27. Measured Air and Electronic Package Temperatures of the Thermosonde.

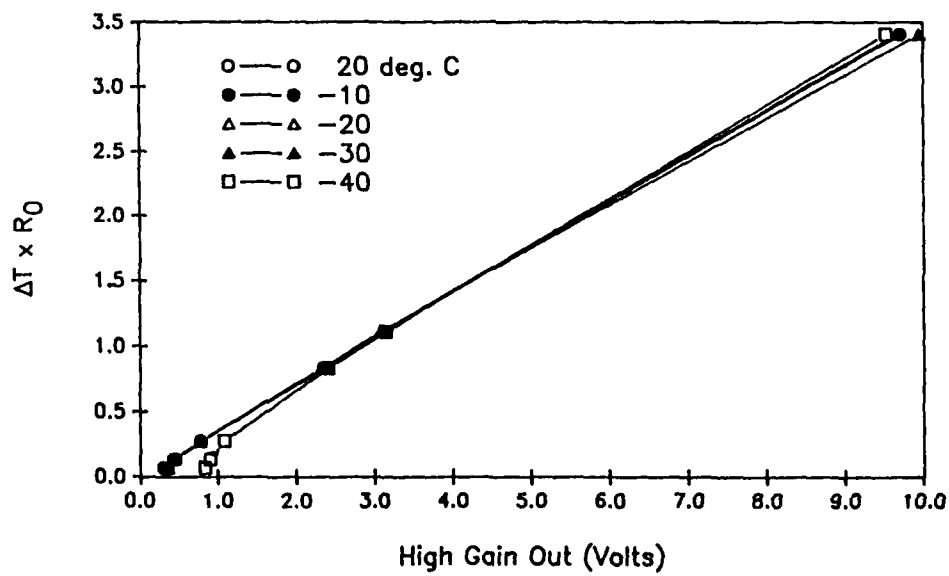
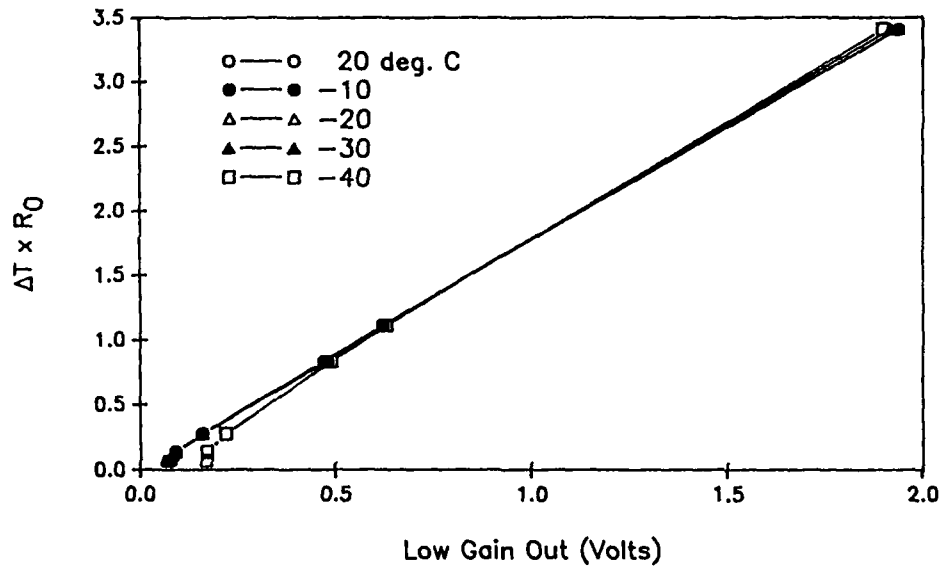


Figure 28. Measured Output Voltages as a Function of Calibrated Input $C_T \times R_0$ and Temperature in a Laboratory Chamber.

6. CONCLUSIONS

Thermosonde data reveals a diurnal daytime shift in measured levels of C_n^2 in the free atmosphere. The shift is manifested in two ways. First an apparent offset in the smallest measured values of C_n^2 exists. Secondly, the curve of the average profile shows an enhancement over nighttime profiles. Related optical and radar measurements have indicated that differences between day and night probably exist, but because of limited instrumental resolution and altitude capabilities those results are inconclusive.

Several hypothesis have been put forward in this paper concerning possible instrumental or solar based sources of data contamination. We have examined the possibility that solar radiation causes probe heating with subsequent instrumental effects. Calculation, computer simulations, and direct measurements have shown that the sun heats the body of the probe sensor a couple of degrees above the ambient and that the level of heating depends upon the solar aspect angle and magnitude and direction of air flow over the probe. Small number statistics have also indicated some correlation between the solar angle and the baseline shift. However, additional calculations, turbulence simulations, in-situ measurements, and direct laboratory experiments do not support the instrumental data contamination hypothesis. A small but insignificant AC type effect can result from improper probe geometry or probe match together with a coupling of solar heating with velocity turbulence. Transient and DC type effects can occur, but measured, processed, and transmitted root mean square C_n^2 information is not likely to contain instrumental contamination.

The cause of the diurnal variation remains under active investigation. Research is continuing on the likelihood that a layering structure in the ozone or aerosol profile could induce localized heating, instability, and "temperature" turbulence.

References

1. Brown, J.H., Good, R.E., Bench, P.M., Faucher, G., Sonde Experiments for Comparative Measurements of Optical Turbulence, AFGL-TR-82-0079, 24 February 1982. ADA118740
2. Brown, J.H., and Good, R.E., Thermosonde and UHF Radar Measurements of C_n^2 at Westford, Massachusetts (Appendix) – July 1981, AFGL-TR-84-0109, 23 February 1981. ADA145398
3. Morrissey, J. (1972) Atmospheric Temperature Measurements Using Balloons and Rockets, *Temperature Measurements, Geophysical and Astrophysical Temperature Measurements*, Instrument Society of America, **209**: 2299-2311.
4. McAdams, W. (1942) *Heat Transfer*; McGraw-Hill, 2nd ed., 1942.
5. Jakob, M. (1949) *Heat Transfer*, John Wiley and Sons, Inc., 1949.
6. Sucec, J. (1975) *Heat Transfer*, Simon and Schuster (Tech Outlines), 1975.
7. Hilpert, R. (1933) *Forsch. Geb. Ingenieurw.*, **4**:215-224, 1933
8. NOAA, NASA, and USAF (1976) *U.S. Standard Atmosphere, 1976*, U.S. GPO, Washington, D.C.
9. Champaign, F., Sleicher, C., and Wehrmann, O. (1967) *J. Fluid Mech.*, **28**:153-175.
10. Bullock, K., and Bremhorst, K. (1969) *IEEE Transactions on Instruments and Measurements*, **IM-18**: 163-166, 1969.
11. Morgan, V., The Overall Convective Heat Transfer from Smooth Circular Cylinders, *Advances in Heat Transfer*, **11**, Irvine, T. and Hartnett, J., 1975. Bullock, et. al., 1969, were misquoted and the number, 4.5×10^{-3} was given in place of 4.5×10^{-4} .

References

12. Jakob, M. (1949) *Heat Transfer*, Vol. 1, p559, fig. 26-4, John Wiley and Sons, 1949.
13. Smart, W. (1960) *Textbook on Spherical Astronomy*, Cambridge Univ. Press, 4th ed.
14. Slocum, J. (1980) *Celestial Navigation with a Pocket Calculator*, Basic Science Press.
15. Tatarski, V.I. (1961) *Wave Propagation in a Turbulent Medium*, McGraw-Hill, 1961.
16. Morony, M., (1951) *Facts and Figures*, Penguin Books, Ltd., 1951.
17. Burlington, R., and May, D. (1953) *Handbook of Probability and Statistical Tables*, Handbook Pub., Inc., Ohio, 1953.
18. A regression on the $\cos \Theta$ gave no correlation. This results favors the probe heating rather than the atmospheric heating interpretation.
19. (degrees of freedom)
20. Nastrom, G., Gage, K., Balsley, B., *Optical Engineering*, **21**:347, 1982. These authors report radar observations of diurnal variations of C_n^2 of 3 to 10 dB in the stratosphere.
21. Good, R.E., Watkins, B.J., Quesada, A.F., Brown, J.H., and Loriot, G.B., (1982) Radar and Optical Measurements of C_n^2 , *Applied Optics*, **21**:3373-3376.
22. Brown, J.H., and Good, R.E. (1984) *Thermosonde and UHF Radar Measurements of C_n^2 at Westford, Massachusetts— July 1981*, AFGL-TR-84-0109, ADA145398
23. Eaton, F.D., et. al. (1988) Comparisons of VHF Radar, Optical, and Temperature Fluctuation Measurements of C_n^2 , r_0 , and Θ_0 , *Theor. Appl. Climatol.*, **39**:17-29, 1988.

References

24. Warnock, J.M., et. al. (1989) Comparison Among Clear-Air Radar, Thermosonde, and Optical Measurements and Model Estimates of C_n^2 in Very Flat Terrain Over Illinois, Middle Atmospheric Program, *MAP Handbook*, Volume 28, 1989.
25. Eaton, F., et. al. (1989) Comparisons of the Transverse Coherence Length and Isoplanatic Angle Measurements Taken with the Flatlands VHF Radar, Optical Techniques, and Thermosondes, *OE/LASE 89 SPIE Symposium, Proceedings*, April 1989.
26. Jakob, M. (1949) *Heat Transfer*, **1**, p213, eqs. 11-18, John Wiley and Sons, Inc., 1949.
27. Sheldahl Corp. part number 7SG400800-010, specification number G400800.
28. Murphy, G.P. (1981) *New Techniques and Devices for Measuring Stratospheric Winds and Turbulence*, AFGL-TR-81-0128, ADA102680
29. Brown, J.H., et. al. (1982) *Sonde Experiments for Comparative Measurements of Optical Turbulence*, AFGL-TR-82-0079, ADA118740
30. Hills, R.S. (1982) *Research, Design and Development Study to Measure Atmospheric Optical Turbulence*, AFGL-TR-82-0334, ADA123392

Appendix

As noted in the text, the incident solar radiation on the thermosonde probe support was treated as a constant ($f = 0.9$ at 30 km). For purposes of examining the validity of this assumption, the altitude and solar angle dependence of incident solar flux was calculated using ONTAR PCTTRAN7 and the US Standard Atmosphere on a Zenith Z248 computer. Probe heating comparisons between use of constant versus actual atmospheric absorption is thus possible. Figure A1 illustrates the dependence of ΔT on altitude at 15 and 25 km and on solar angle from 20 to 80 degrees. Clearly, compensation for actual transmission introduces little deviation in the probe heating calculations. Solar heating calculations for the black, white, and stainless steel probes for constant versus LOWTRAN determined absorption are compared in Figure A2. This graph corresponds to Figure 3 in the text but here illustrates the small (but insignificant increase in ΔT for actual conditions of absorption. Linear regression curves of the $\langle C_T^2 \rangle$ baseline shift with ΔT for constant versus LOWTRAN calculated absorption are illustrated in Figure A3. This graph corresponds to Figure 9 in the text but demonstrates that only slight corrections are introduced by actual absorption. The approximation that solar flux is constant at the probe is thus justified based on a fuller consideration of atmospheric transmission as determined by LOWTRAN 7.

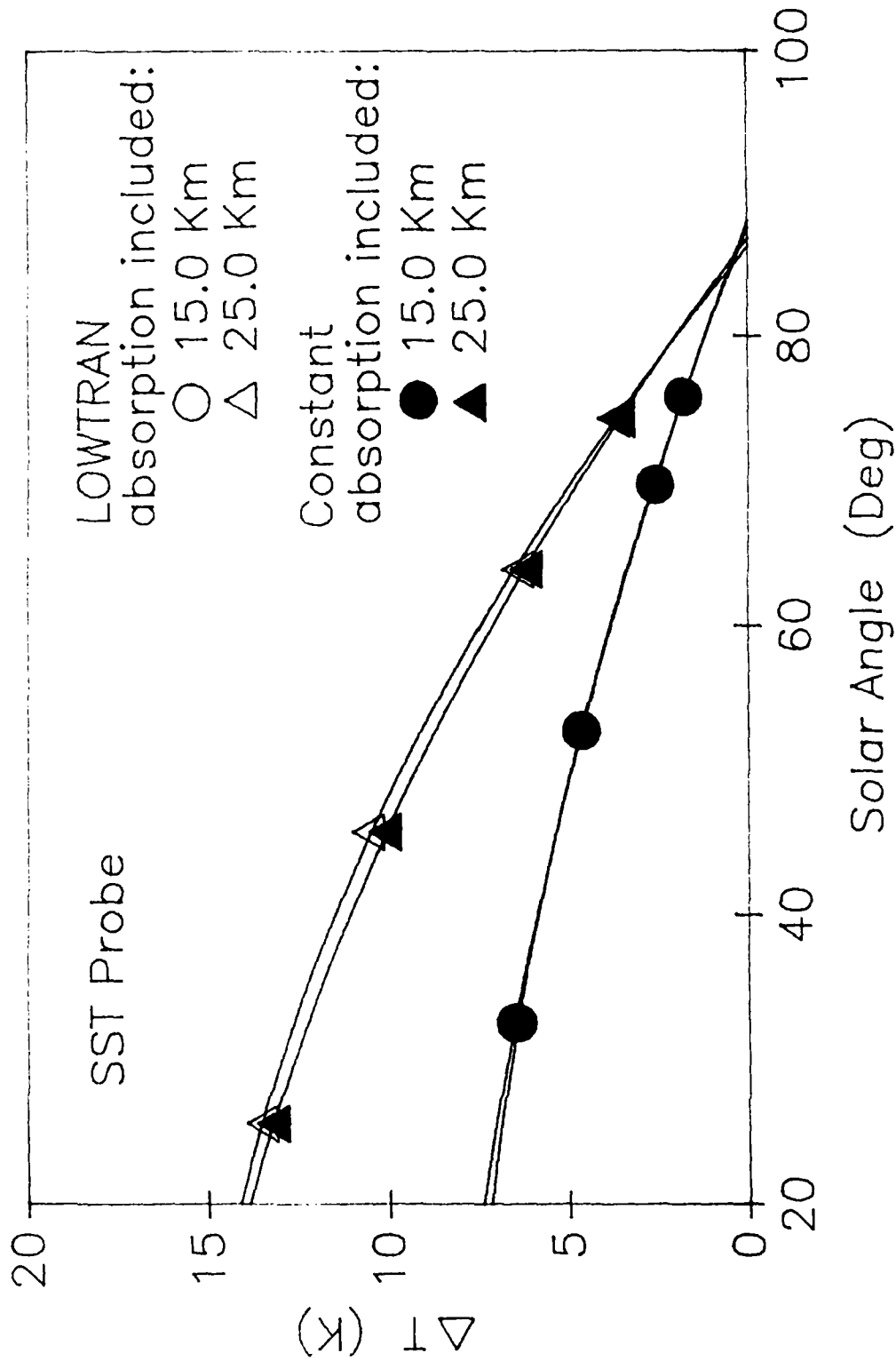


Figure A1. Dependence of ΔT on Altitude and Solar Angle.

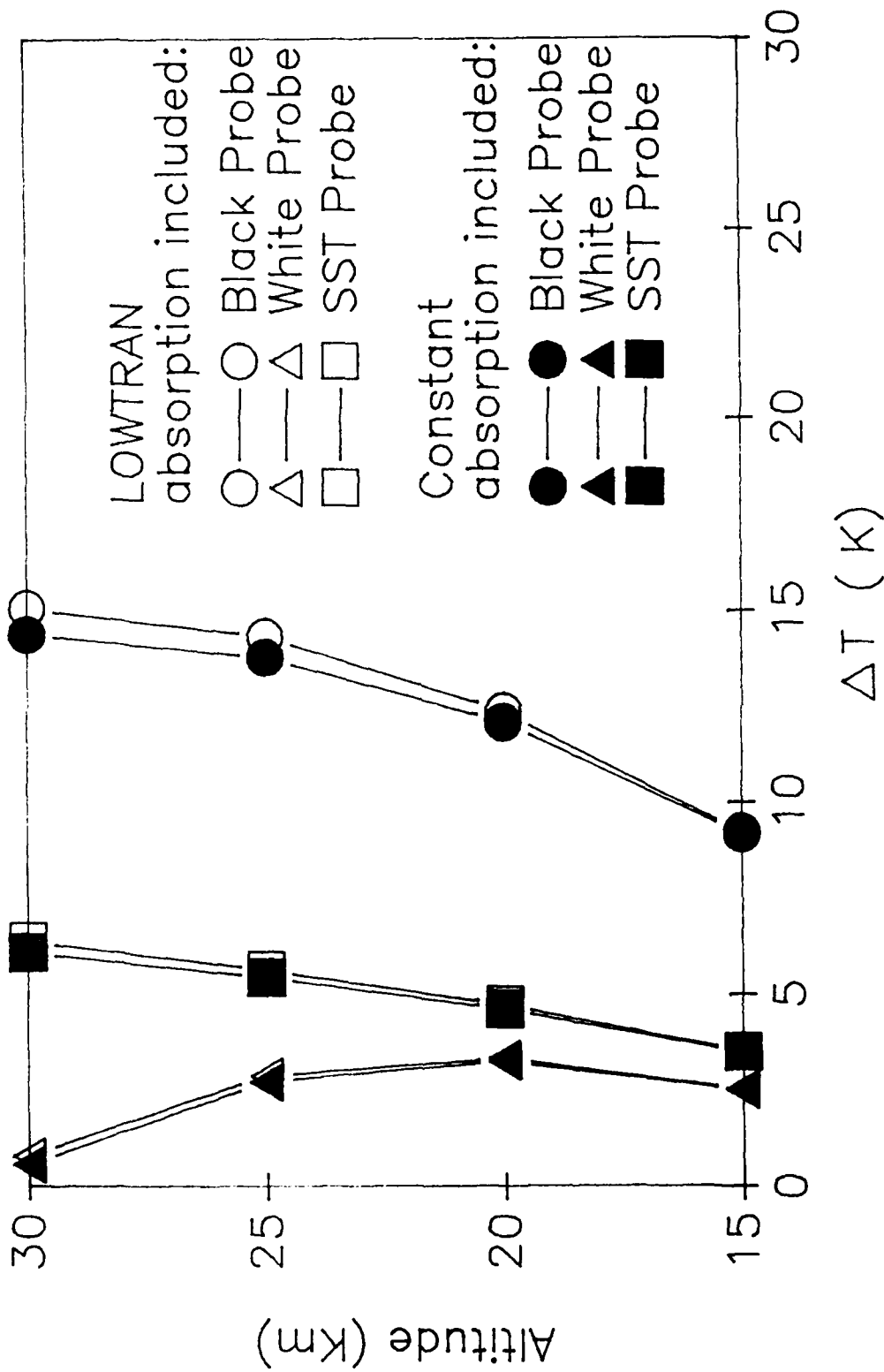


Figure A2. ΔT vs Altitude for Black, White, and Stainless Steel Probes, for LOWTRAN absorption and for constant absorption.

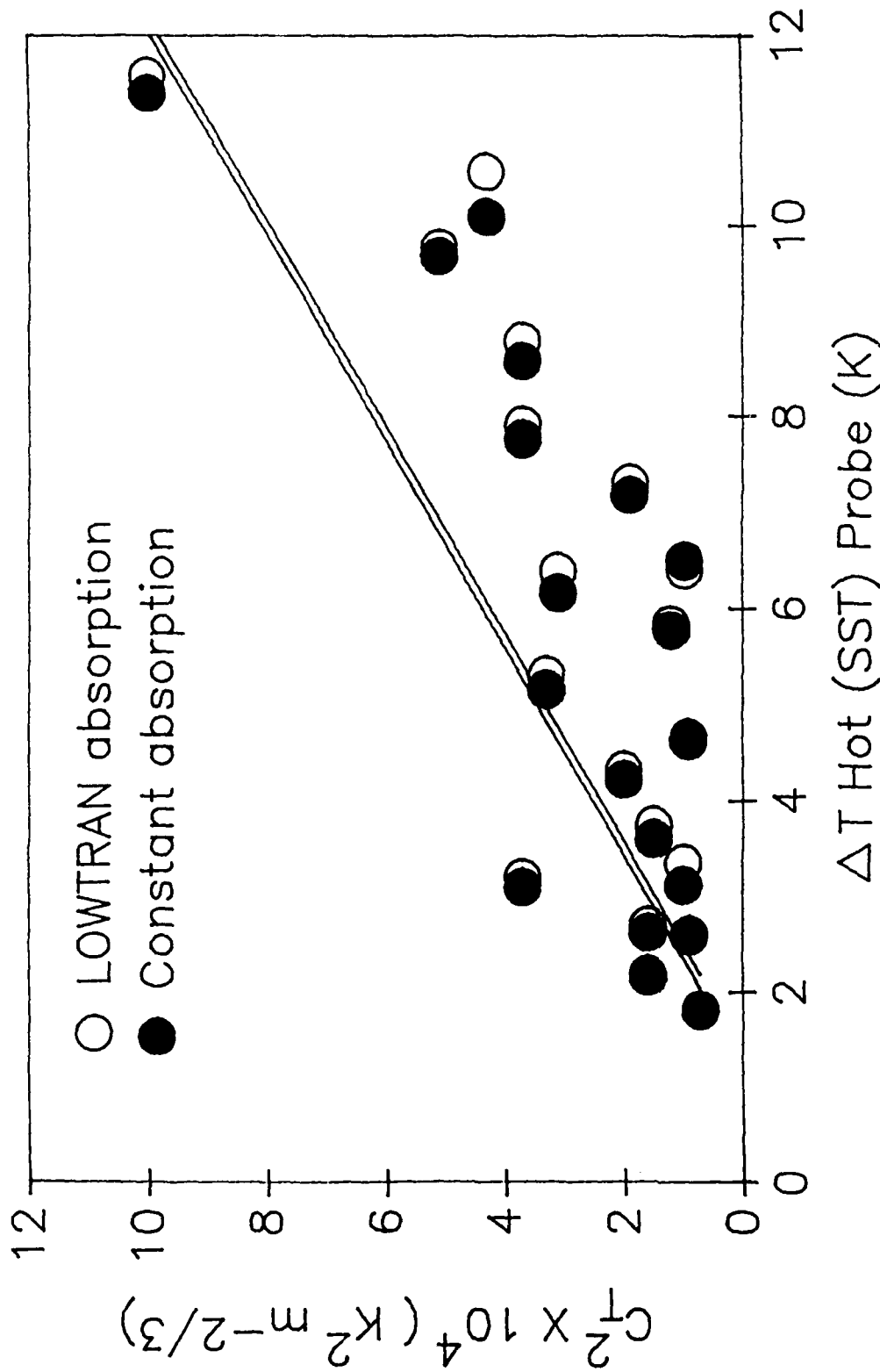


Figure A3. Baseline Shifts -- ΔT for LOWTRAN and Constant Absorption.